SUPPORTING INFORMATION

Mechanical Interlocking of SWNTs with N-rich Macrocycles for Efficient ORR Electrocatalysis.

Wanzheng Zhang, Melanie Guillén-Soler, Sara Moreno-Da Silva, Alejandro López-Moreno, Luisa R. González, Maria del Carmen Giménez-López, and Emilio M. Pérez

Chemical and reagents

Reagents were obtained from Sigma-Aldrich or TCI Chemicals and used without further purification. (6,5)-SWNTs (≥ 95% carbon basis (≥ 95% as carbon nanotubes), 0.78 nm average diameter) and (7,6)-SWNTs (≥ 90% carbon basis (≥77% as carbon nanotubes), 0.83 nm average diameter) were obtained from Sigma-Aldrich. Solvents were dried following standard procedures. Air-sensitive reactions were carried out under argon atmosphere. Analytical thin layer chromatographies (TLC) were performed using aluminium-coated Merck Kiesel silica gel 60 F254 plates or aluminium-coated Macherey-Nagel aluminium oxide F254 plates. Column chromatography purification was performed using silica gel (Scharlau 60, 70-230 mesh) or aluminium oxide (Merck, Kieselgel 60, 230-240 mesh).

Equipment

Nuclear Magnetic Resonance - NMR NMR spectra were recorded on a BrukerAvance 400 (^{1}H: 400 MHz; COSY: 400 MHz; ^{13}C 101 MHz) at 298K, using partially deuterated solvents as internal standards. Coupling constants (J) are denoted in Hz and chemical shifts (δ) in ppm. Multiplicities are denoted as follows: s = singlet, d = doublet, t = triplet, m = multiplet, b = broad, dd = doublet of doublets.

Thermogravimetric Analyses - TGA Thermogravimetric analyses were performed using a TA Instruments TGAQ500 with a ramp of 10 °C/min under air and nitrogen conditions from 100 to 1000 °C.

Raman spectroscopy - Raman spectra were recorded with a Bruker Senterra confocal Raman microscope (Bruker Optic, Ettlingen, Germany, resolution 9-15 cm^{-1}).

Ultraviolet/Visible/Near Infrared Spectroscopy – UV/VIS/NIR Spectroscopy UV-vis-NIR spectra were performed using a Cary 5000 UV/Vis/NIR spectrophotometer (Varian) and 10x10 mm quartz cuvettes (path length = 1 cm).

Mass Spectrometry Fast atom bombardment (FAB) matrix-assisted laser desorption ionization (coupled to a Time-Of-Flight analyser) (MALDI-TOF), and electrospray ionization (ESI) experiments were recorded on a VG AutoSpec spectrometer,a Bruker REFLEX spectrometer, and a Bruker MAXIS II, respectively.

Atomic Force Microscopy (AFM) images were acquired using a JPK NanoWizard II AFM working in dynamic mode coupled to an inverted optical microscope Nikon Eclipse Ti-U. NT-MDT NSG01 silicon cantilevers, with typical values of 5.1 N·m–1 spring constant and 150 kHz resonant frequency, were employed under ambient conditions in air. The samples were dispersed in tetrachloroethane and spin coated onto mica slides.

Transmission electron microscopy (TEM) images were obtained in a JEOL-JEM 2100F (2.5 Å resolution) instrument operating at 200 kV. High resolution-transmission electron microscopy (HR-TEM) images were obtained in an imaging aberration corrected microscope JEOL JEM GRAND ARM300cF operating at 60 kV. Images were recorded on a slow-CCD camera GATAN Oneview. Approximately 0.2 mg of MINT was ultrasonic dispersed in 2 mL of tetrachloroethane for ten minutes. Few drops of this dispersion were deposited onto a 200 square mesh grid covered by holey carbon. After solvent evaporation in air, the grid was ready to use.

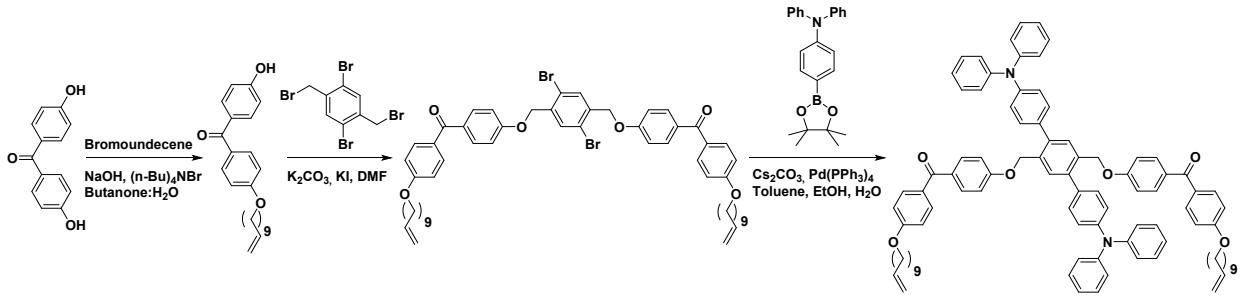

(4-hydroxyphenyl)(4-(undec-10-en-1-yloxy)phenyl)methanone.

4,4'-Dihydroxybenzophenone (5 g, 23.3 mmol), tetrabutylammonium bromide (3.9 g, 12 mmol) and sodium hydroxide (0.96 g, 24 mmol) were dissolved in a mixture of water/butanone (80 mL / 80 mL), and Subsequently 11-bromo-1-undecene (5.6 g, 24 mmol) was added. The reaction was stirred for 1 hour at 85 °C.The crude reaction was poured into 1 M aqueous HCl and extracted with ethyl acetate. The organic phase was washed with water, dried over $MgSO_4$, filtered and solvents were removed by evaporation under vacuum. The resulting product subjected to column chromatography (Ethyl acetate/CH_2Cl_2 1:20) to obtain the pure product (2.28 g, 27 %) as a white solid. ^{1}H NMR (400 MHz, $CDCl_3$, ppm) δ 7.70 (d, *J* = 8.8 Hz, 2H), 7.64 (d, *J* = 8.4 Hz, 2H), 6.86 (dd, *J* = 8.6, 2.0 Hz, 4H), 5.78 - 5.68, (m, 1H), 4.93 - 4.84, (m, 2H), 3.94 (t, *J* = 6.4 Hz, 2H), 1.99 - 1.94 (m, 2H), 1.76 - 1.69 (m, 2H), 1.40 - 1.23 (m, 12); ^{13}C NMR (101 MHz, $CDCl_3$, ppm) δ 195.9, 162.8, 160.6, 139.2, 132.8, 132.6, 130.2, 130.0, 115.3, 114.2, 114.0, 68.3, 33.8, 29.5, 29.4, 29.4, 29.1, 28.9, 26.0; HRMS (ESI) m/z calc. for $C_{24}H_{31}O_3$ $[M+H]^+$: 367.2268; found 367.2270.

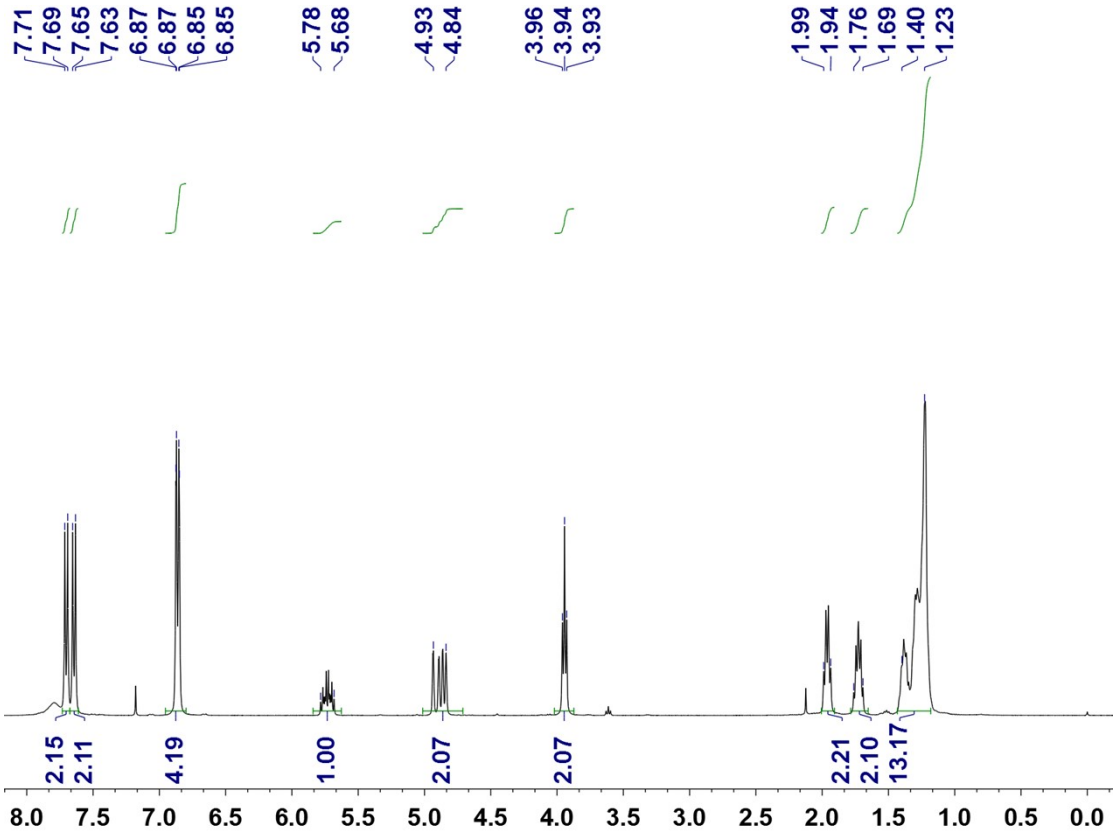
7.71
7.69
7.65
7.63
6.87
6.87
6.85
6.85
5.78
5.68
4.93
4.84
3.96
3.94
3.93
1.99
1.94
1.76
1.69
1.40
1.23
2.15
2.11
4.19
1.00
2.07
2.07
2.21
2.10
13.17
8.0
7.5
7.0
6.5
6.0
5.5
5.0
4.5
4.0
3.5
3.0
2.5
2.0
1.5
1.0
0.5
0.0

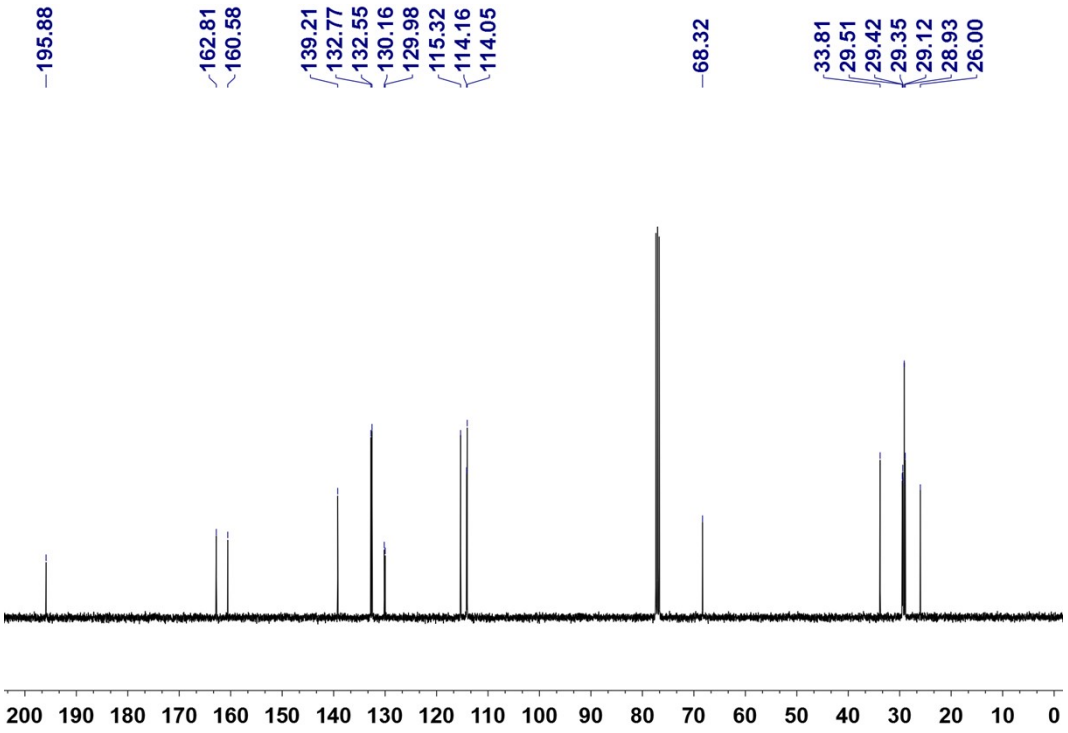
195.88
162.81
160.58
139.21
132.77
132.55
130.16
129.98
115.32
114.16
114.05
68.32
33.81
29.51
29.42
29.35
29.12
28.93
26.00
200
190
180
170
160
150
140
130
120
110
100
90
80
70
60
50
40
30
20
10
0

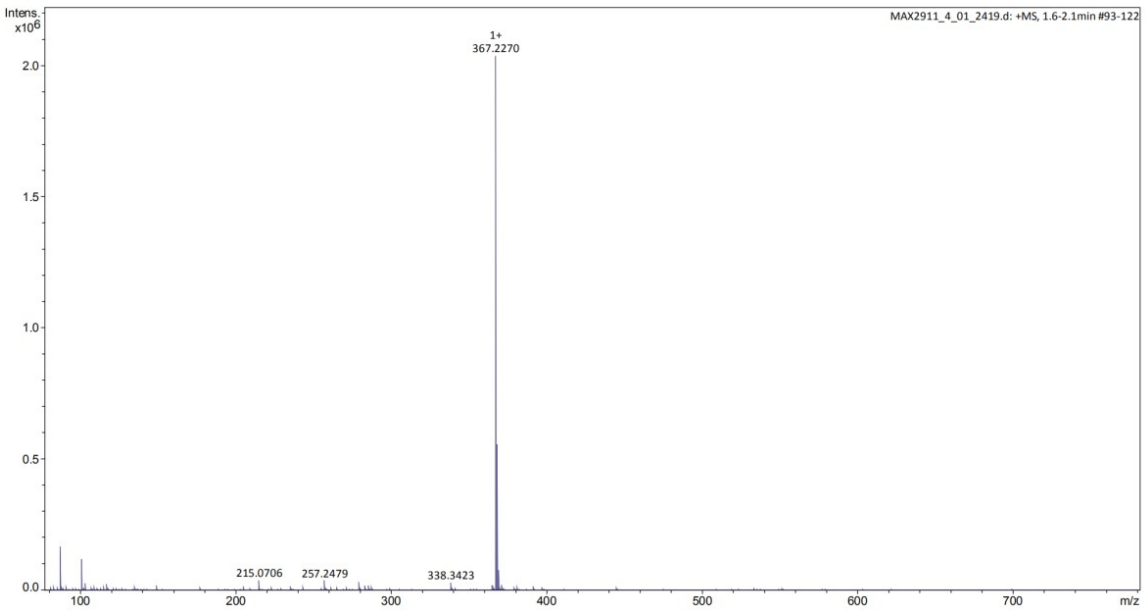

((((2,5-dibromo-1,4-phenylene)bis(methylene))bis(oxy))bis(4,1-phenylene))bis((4-(undec-10-en-1-yloxy)phenyl)methanone)

Potassium carbonate (0.7 g, 5 mmol), a catalytic amount of potassium iodide and 1,4-bis-bromomethyl-benzene (0.84 g, 2 mmol) were added to a solution of (4-hydroxyphenyl)(4-(undec-10-en-1-yloxy)phenyl)methanone (1.83 g, 5 mmol) in 30 mL dry N, N-dimethylformamide (DMF). The reaction was stirred for 20 hours at 80 °C under nitrogen (N_2). The crude reaction was poured into 1 M aqueous HCl and extracted with ethyl acetate. The organic phase was washed with water, dried over $MgSO_4$, filtered and solvents were removed by evaporation under vacuum. The resulting product subjected to column chromatography ($CHCl_3$) to obtain the pure product (0.55 g, 28 %) as a pale yellow solid. ^{1}H NMR (400 MHz, $CDCl_3$, ppm) δ 7.85 - 7.80 (m, 10H), 7.08 (d, *J* = 8.8 Hz, 4H), 6.97 (d, *J* = 8.8 Hz, 4H), 5.89 - 5.79 (m, 2H), 5.20 (s, 4H), 5.04 - 5.94 (m, 4H), 4.06 (t, *J* = 6.4 Hz, 4H), 2.10 - 2.04 (m, 4H), 1.88 - 1.78 (m, 4H), 1.53 -1.33 (m, 24H); ^{13}C NMR (101 MHz, $CDCl_3$, ppm) δ 194.3, 162.6, 161.1, 139.2, 137.2, 132.4, 132.3, 132.3, 131.7, 130.3, 121.2, 114.3, 114.2, 114.0, 68.7, 68.3, 33.81, 29.5, 29.4, 29.4, 29.1, 29.1, 28.9, 26.0; HRMS (ESI) m/z calc. for $C_{56}H_{65}O_6Br_2$ $[M+H]^+$: 991.3141; found 991.3146.

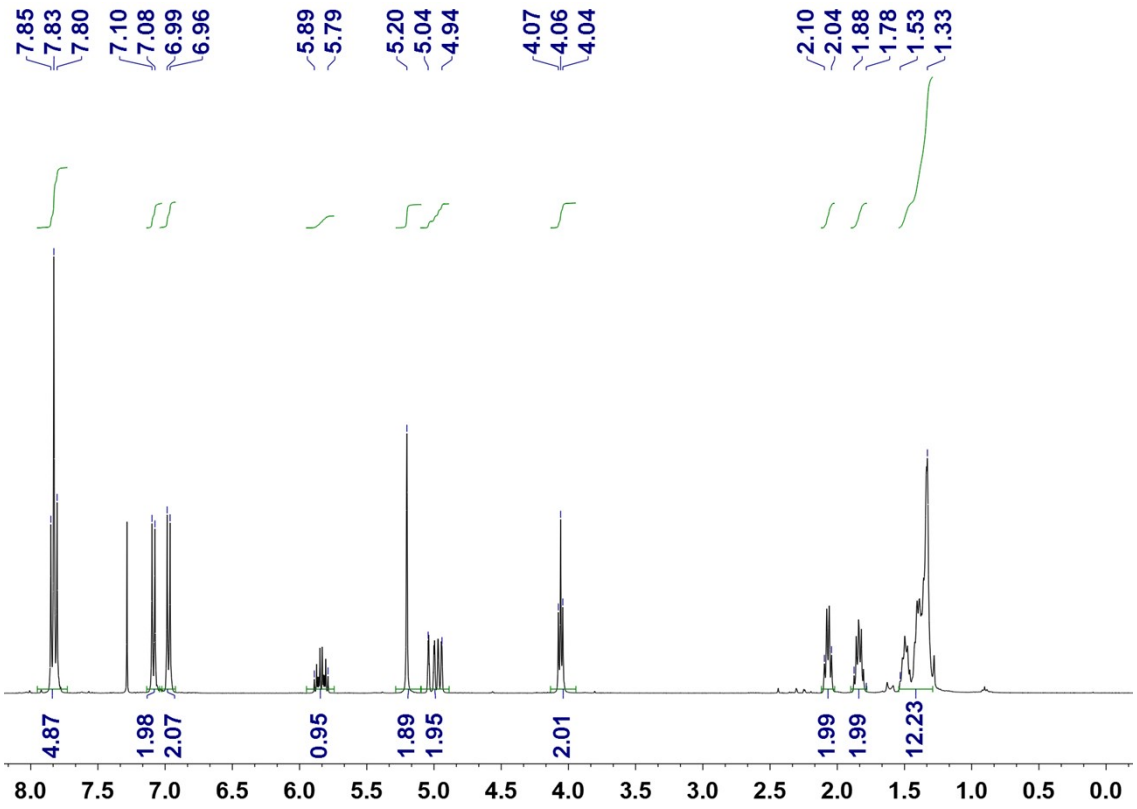
7.85
7.83
7.80
7.10
7.08
6.99
6.96
5.89
5.79
5.20
5.04
4.94
4.07
4.06
4.04
2.10
2.04
1.88
1.78
1.53
1.33
4.87
1.98
2.07
0.95
1.89
1.95
2.01
1.99
1.99
12.23
8.0 7.5 7.0 6.5 6.0 5.5 5.0 4.5 4.0 3.5 3.0 2.5 2.0 1.5 1.0 0.5 0.0

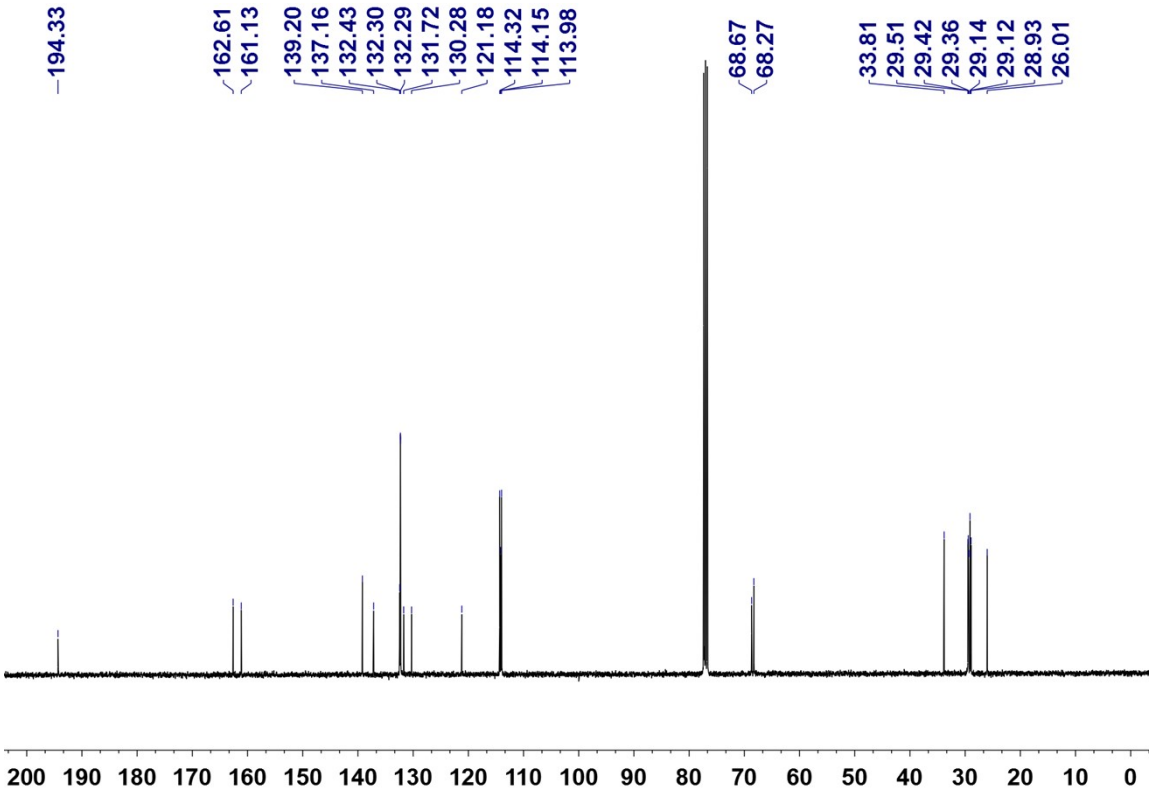
194.33
162.61
161.13
139.20
137.16
132.43
132.30
132.29
131.72
130.28
121.18
114.32
114.15
113.98
68.67
68.27
33.81
29.51
29.42
29.36
29.14
29.12
28.93
26.01
200 190 180 170 160 150 140 130 120 110 100 90 80 70 60 50 40 30 20 10 0

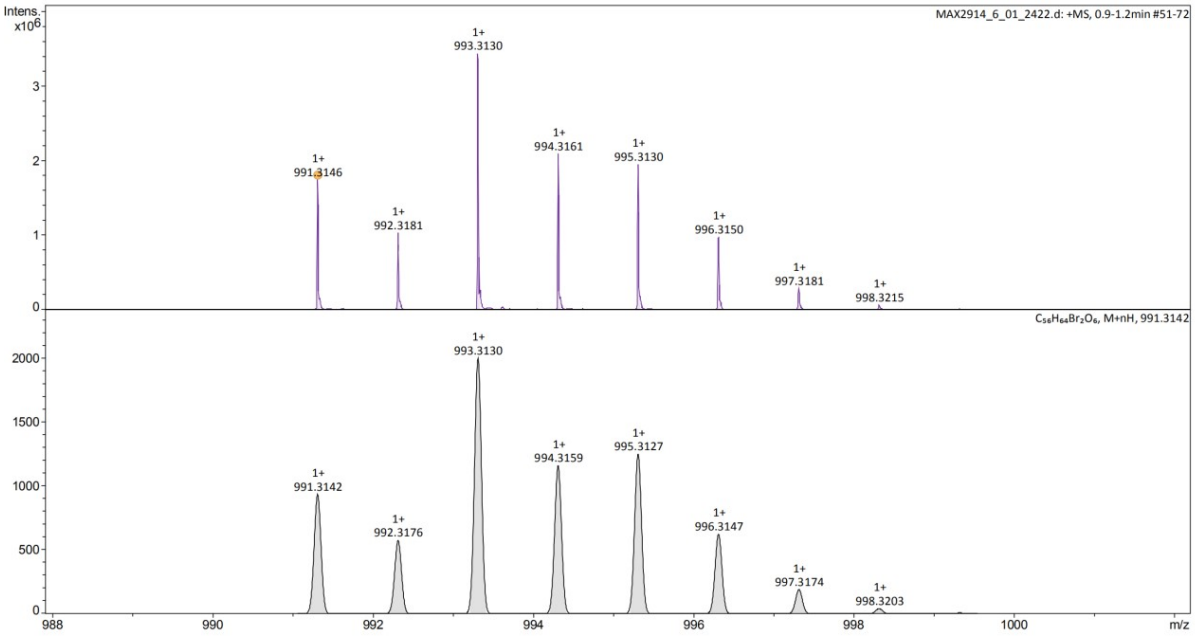

((((4,4''-bis(diphenylamino)-[1,1':4',1''-terphenyl]-2',5'-diyl)bis(methylene))bis(oxy))bis(4,1-phenylene))bis((4-(undec-10-en-1-yloxy)phenyl)methanone).

((((2,5-dibromo-1,4-phenylene)bis(methylene))bis(oxy))bis(4,1-phenylene))bis((4-(undec-10-en-1-yloxy)phenyl)methanone) (218 mg, 0.22 mmol), 4-(Diphenylamino)phenylboronic acid pinacol ester (200 mg, 0.54 mmol), Cs_2CO_3 (180 mg, 0.55 mmol), and $Pd(PPh_3)_4$ (28 mg, 0.024 mmol) were added to a mixture of toluene / ethanol / water (30 / 9 / 9 ml) and bubbled with nitrogen (N_2) for 15 minutes. The reaction was stirred for 15 hours at 90 °C under nitrogen (N_2). The crude reaction was poured into water and extracted with ethyl acetate. The organic phase was washed with water, dried over $MgSO_4$, filtered and solvents were removed by evaporation under vacuum. The resulting product subjected to column chromatography (CH_2Cl_2) to obtain the pure product (271 mg, 93 %) as a white solid. ^{1}H NMR (400 MHz, $CDCl_3$, ppm) δ 7.68 (dd, *J* = 8.8, 2.4 Hz, 8H), 7.55 (s, 2H), 7.23 - 7.16 (m, 12H), 7.05 - 6.93 (m, 16H), 6.88 - 6.84 (m, 8H), 5.05 (s, 4H), 4.94 -4.84 (m, 4H), 3.95 (t, *J* = 6.0 Hz, 4H), 1.99 - 1.94 (m, 4H), 1.77 - 1.70 (m, 4H), 1.41 - 1.23 (m, 24H); ^{13}C NMR (101 MHz, $CDCl_3$, ppm) δ 194.4, 162.5, 161.8, 147.5, 147.4, 140.9, 139.2, 133.6, 133.2, 132.2, 132.2, 131.4, 131.1, 130.4, 129.9, 129.4, 124.7, 123.2, 122.8, 114.3, 114.2, 113.9, 68.3, 33.8, 29.5, 29.4, 29.4, 29.2, 29.1, 28.9, 26.0; HRMS (ESI) m/z calc. for $C_{92}H_{93}N_2O_6$ $[M+H]^+$: 1321.7028; found 1321.7027.

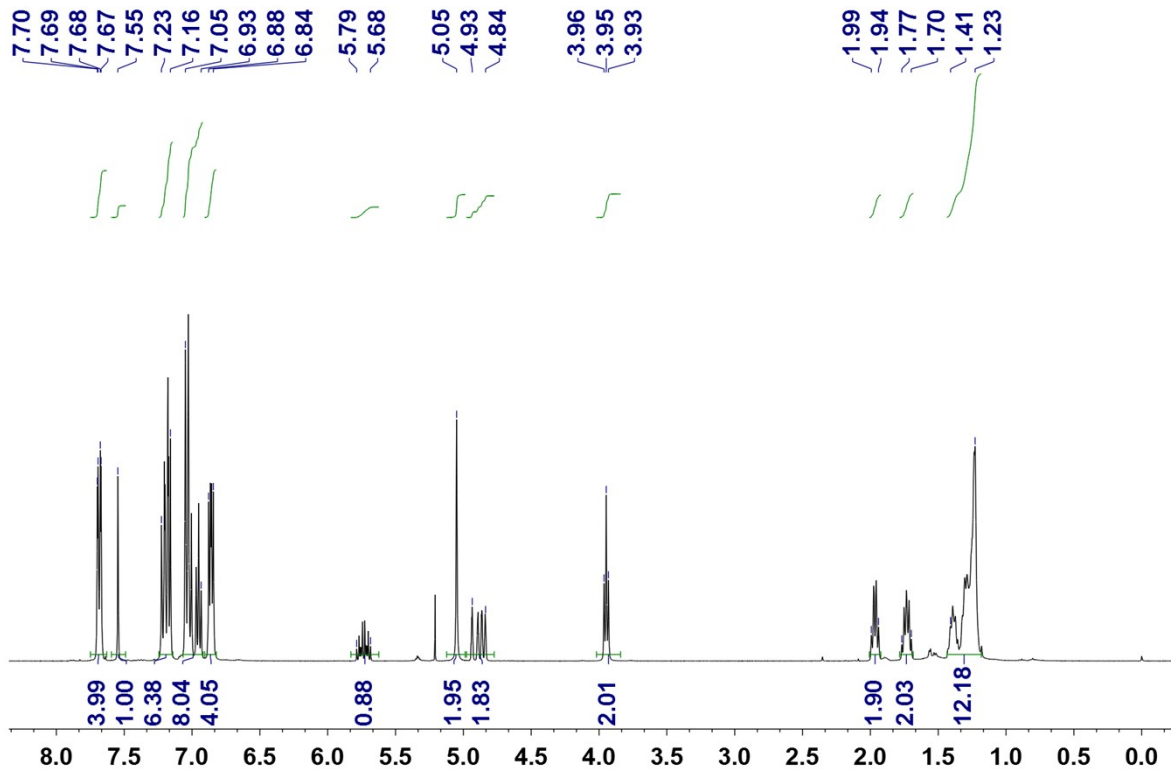
7.70
7.69
7.68
7.67
7.55
7.23
7.16
7.05
6.93
6.88
6.84
5.79
5.68
5.05
4.93
4.84
3.96
3.95
3.93
1.99
1.94
1.77
1.70
1.41
1.23
3.99
1.00
6.38
8.04
4.05
0.88
1.95
1.83
2.01
1.90
2.03
12.18
8.0 7.5 7.0 6.5 6.0 5.5 5.0 4.5 4.0 3.5 3.0 2.5 2.0 1.5 1.0 0.5 0.0

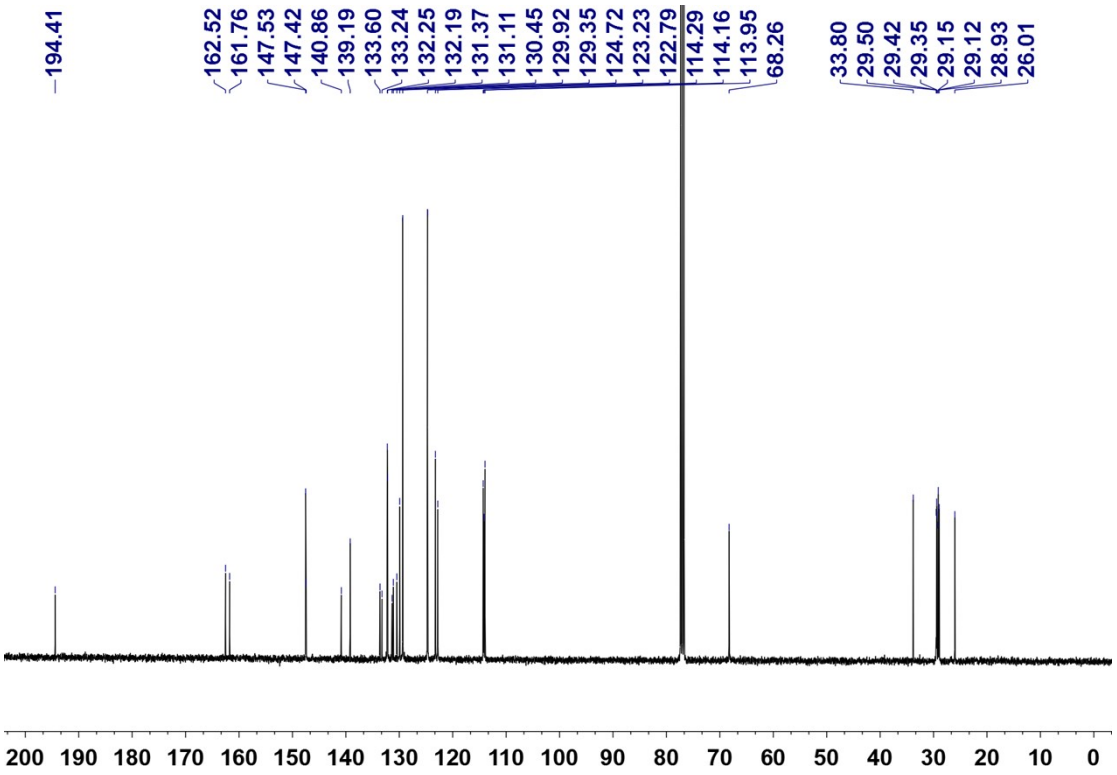
194.41
162.52
161.76
147.53
147.42
140.86
139.19
133.60
133.24
132.25
132.19
131.37
131.11
130.45
129.92
129.35
124.72
123.23
122.79
114.29
114.16
113.95
68.26
33.80
29.50
29.42
29.35
29.15
29.12
28.93
26.01
200 190 180 170 160 150 140 130 120 110 100 90 80 70 60 50 40 30 20 10 0

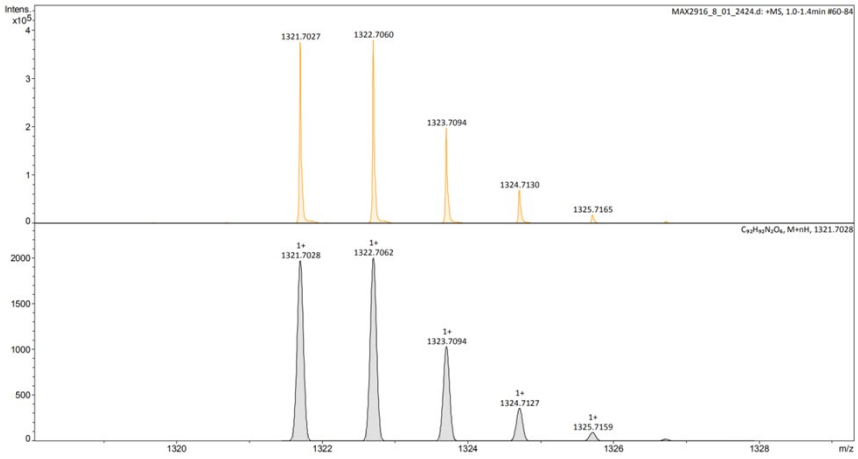

6²,6⁵-bis(4-(diphenylamino)phenyl)-4,8,12,33-tetraoxa-1,3,6,9,11(1,4)-pentabenzenacyclotritriacontaphan-22-ene-2,10-dione

Grubbs' 2nd generation catalyst (3.5 mg, 0.004 mmol) was added to a solution of u-shape (10 mg, 0.0075 mmol) in 30 mL $CHCl_3$. The reaction was stirred under reflux overnight. The organic solvents were removed by evaporation under vacuum. The resulting product subjected to column chromatography (CH_2Cl_2) to obtain the pure product (6 mg, 61 %) as a white solid. ^{1}H NMR (400 MHz, $CDCl_3$, ppm) δ 7.71 - 7.63 (m, 8H), 7.49 (s, 2H), 7.22 - 7.15 (m, 12H), 7.07 - 6.96 (m, 16H), 6.86 - 6.78 (m, 8H), 5.34 - 5.30 (m, 2H), 5.15 (s, 4H), 3.95 (t, J = 6.4 Hz, 4H), 1.94 - 1.88 (m, 4H), 1.76 - 1.70 (m, 4H), 1.40 - 1.19 (m, 24H); ^{13}C NMR (101 MHz, $CDCl_3$, ppm) δ 194.5, 162.4, 161.4, 147.5, 140.4, 133.6, 133.0, 132.2, 132.1, 131.0, 130.6, 130.4, 130.3, 129.9, 129.4, 124.8, 123.3, 122.7, 114.6, 114.3, 113.9, 68.1, 32.6, 29.6, 29.5, 29.4, 29.2, 29.1, 29.0, 25.9; HRMS (ESI) m/z calc. for $C_{90}H_{89}N_2O_6$ $[M+H]^+$: 1293.6715; found 1293.6703.

Comment [A]:

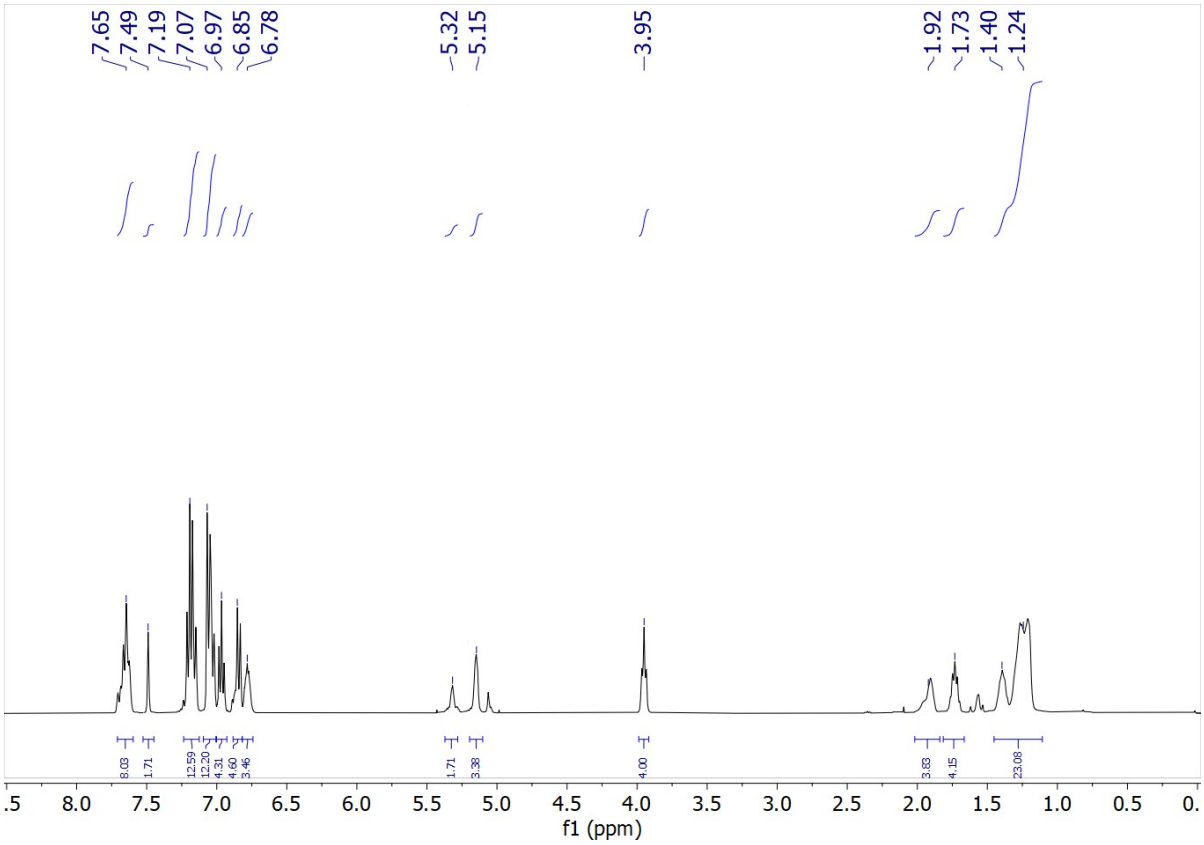
7.65
7.49
7.19
7.07
6.97
6.85
6.78
5.32
5.15
3.95
1.92
1.73
1.40
1.24
8.03
1.71
12.59
12.20
4.31
4.60
3.46
1.71
3.38
4.00
3.83
4.15
23.08
f1 (ppm)

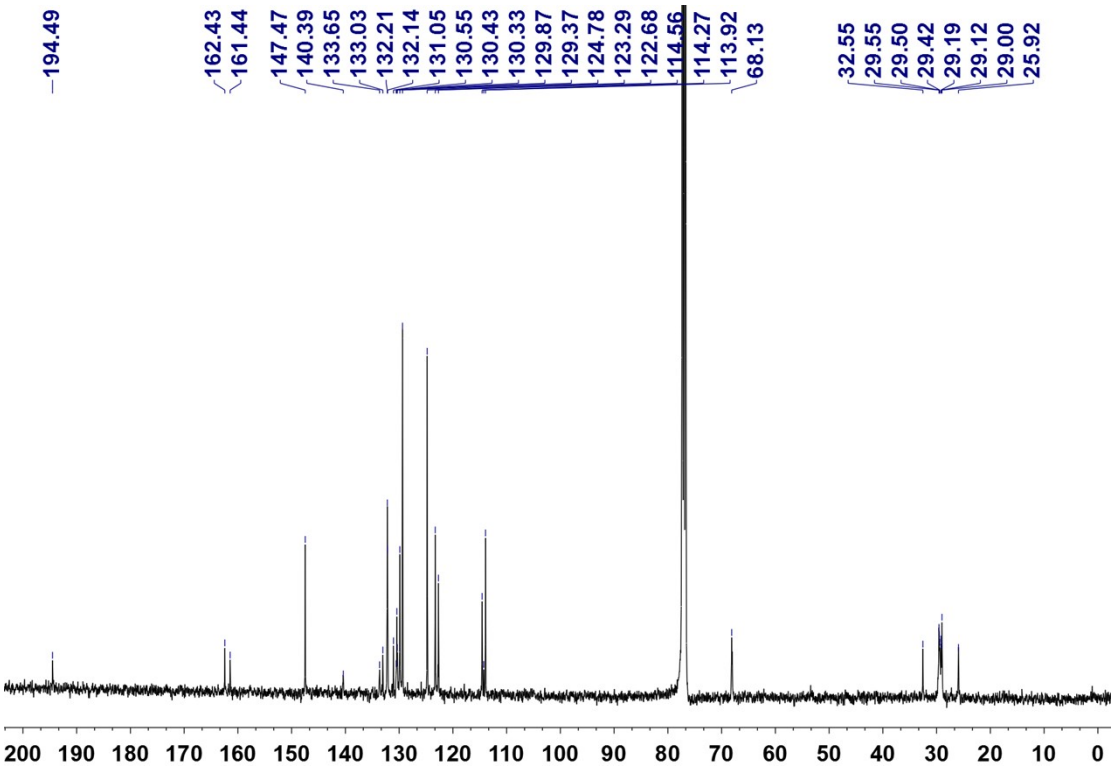
194.49
162.43
161.44
147.47
140.39
133.65
133.03
132.21
132.14
131.05
130.55
130.43
130.33
129.87
129.37
124.78
123.29
122.68
114.56
114.27
113.92
68.13
32.55
29.55
29.50
29.42
29.19
29.12
29.00
25.92

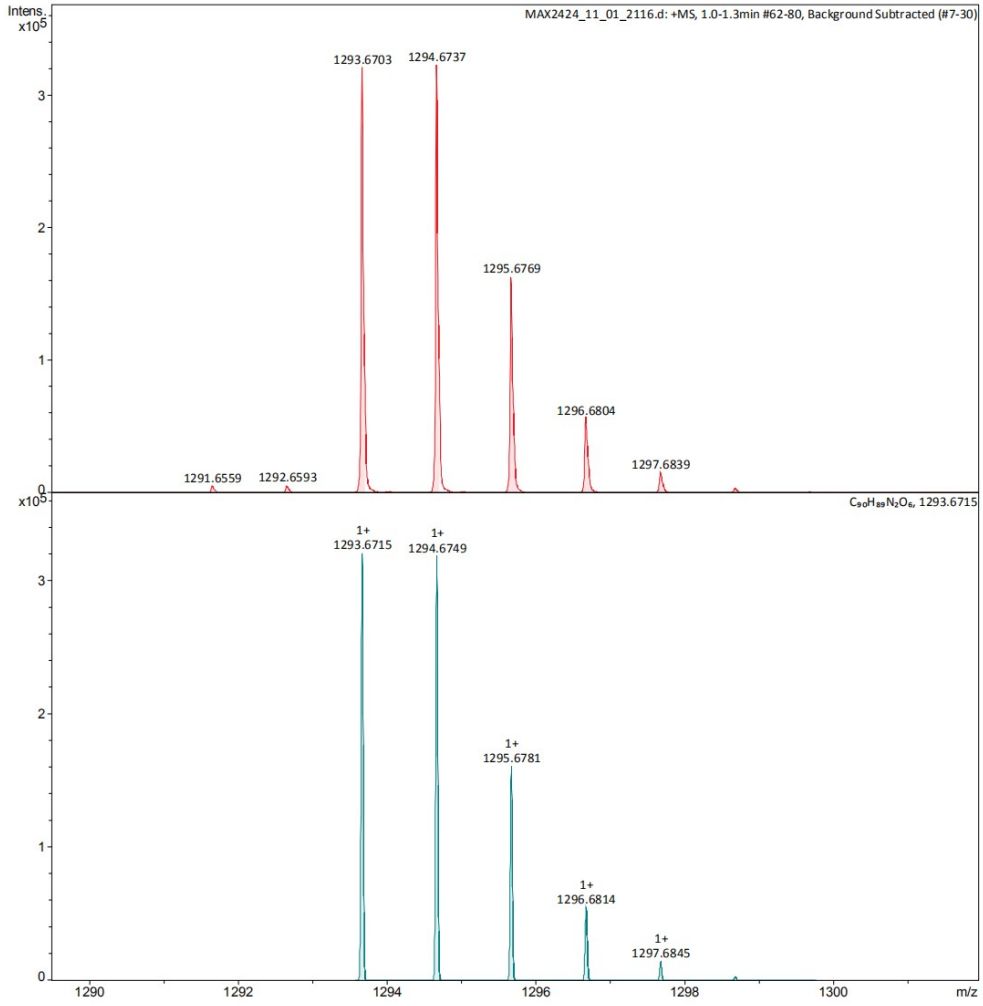

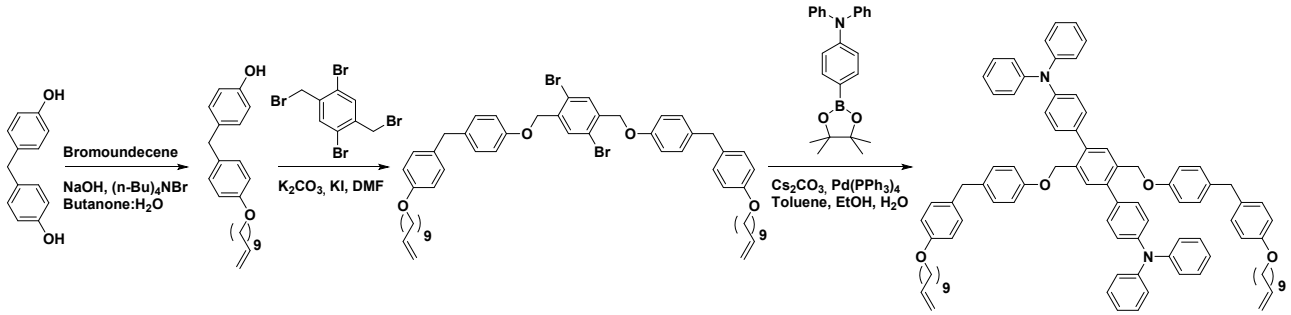

(4-hydroxyphenyl)(4-(undec-10-en-1-yloxy)phenyl)methane.

4,4'-Dihydroxydiphenylmethane (7.5 g, 37.5 mmol), tetrabutylammonium bromide (13 g, 40.4 mmol) and sodium hydroxide (1.5 g, 37.5 mmol) were dissolved in a mixture of water/butanone (90 mL / 90 mL), and Subsequently 11-bromo-1-undecene (9.5 g, 40.8 mmol) was added. The reaction was stirred for 1 hour at 85 °C.The crude reaction was poured into 1 M aqueous HCl and extracted with ethyl acetate. The organic phase was washed with water, dried over $MgSO_4$, filtered and solvents were removed by evaporation under vacuum. The resulting product subjected to column chromatography (CH_2Cl_2) to obtain the pure product (4.8 g, yield, 36.4 %) as a white solid. ^{1}H NMR (400 MHz, $CDCl_3$, ppm) δ 6.99 (d, *J* = 8.8 Hz, 2H), 6.96 (d, *J* = 8.4 Hz, 2H), 6.74 (d, *J* = 8.4 Hz, 2H), 6.66 (d, *J* = 8.4 Hz, 2H), 5.79 - 5.69, (m, 1H), 4.94 - 4.84, (m, 2H), 3.84 (t, *J* = 6.4 Hz, 2H), 3.77 (s, 2H), 1.99 - 1.94 (m, 2H), 1.72 - 1.65 (m, 2H), 1.38 - 1.22 (m, 12);

^{13}C NMR (101 MHz, $CDCl_3$, ppm) δ 157.5, 153.7, 139.2, 133.9, 133.4, 129.9, 129.7, 115.2, 114.5, 114.1, 68.0, 40.1, 33.8, 29.5, 29.4, 29.4, 29.3, 29.1, 28.9, 26.1; HRMS (ESI) m/z calc. for $C_{24}H_{33}O_2$ $[M+H]^+$: 353.2475; found 353.2474.

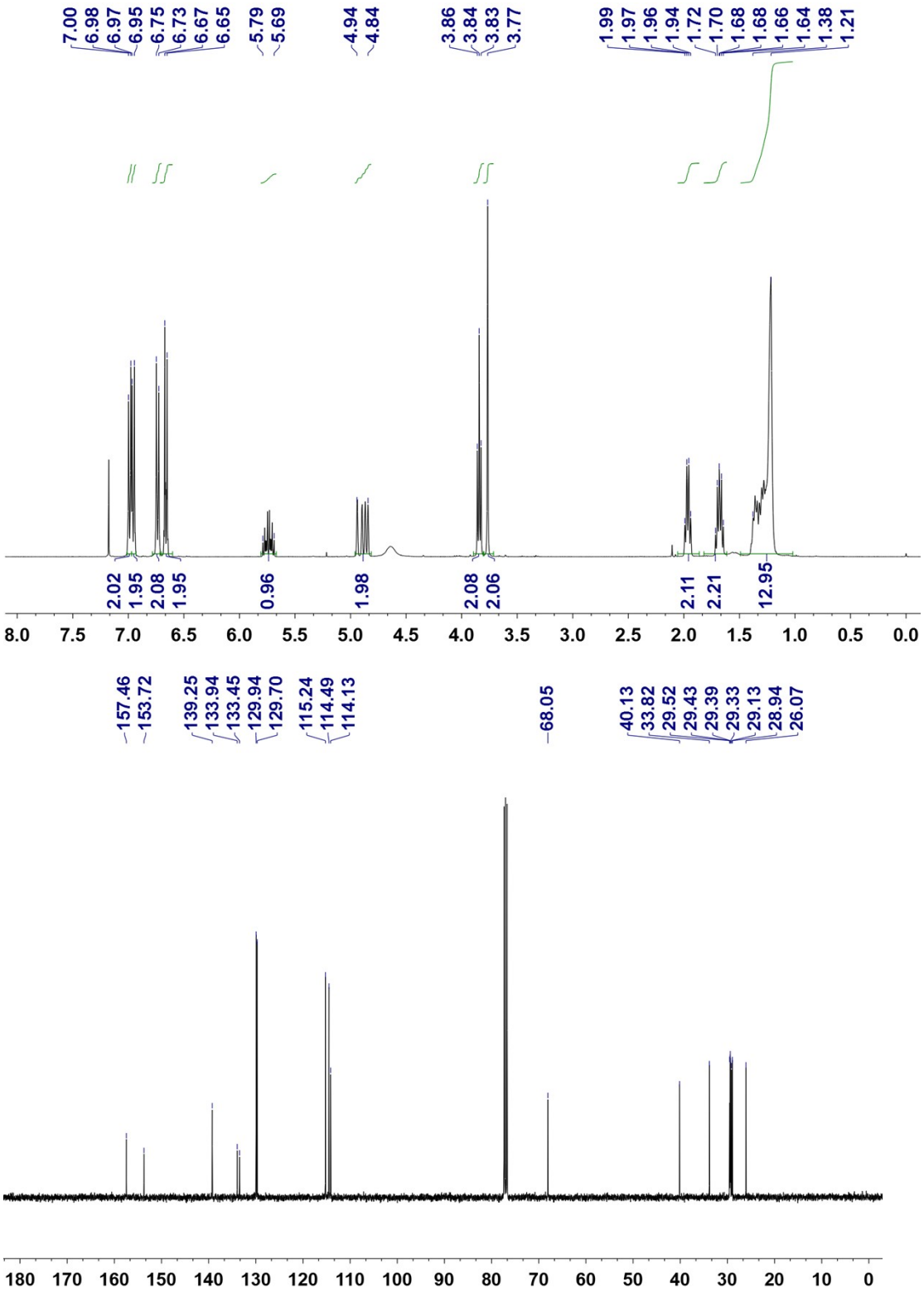

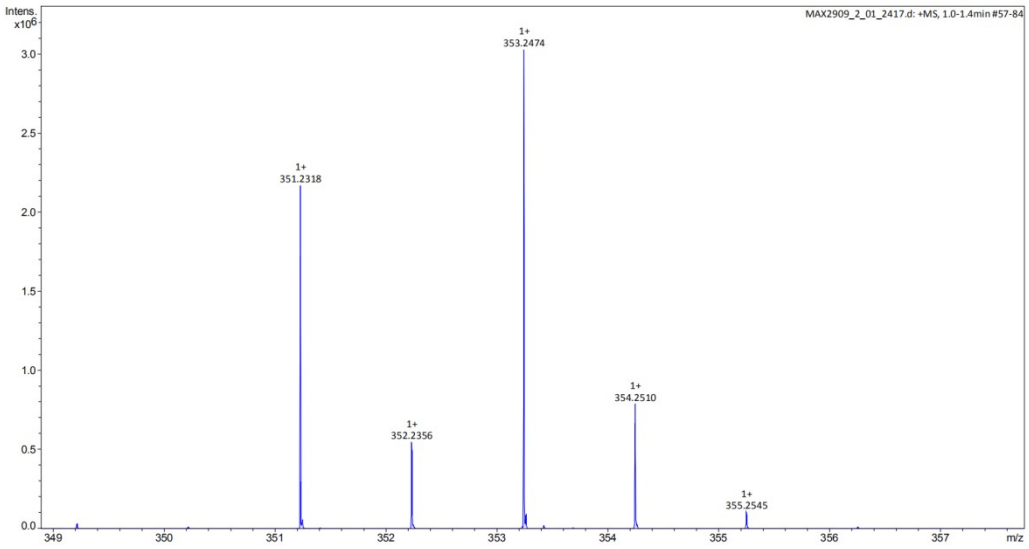

((((2,5-dibromo-1,4-phenylene)bis(methylene))bis(oxy))bis(4,1-phenylene))bis((4-(undec-10-en-1-yloxy)phenyl)methane)

Potassium carbonate (1 g, 7.2 mmol), a catalytic amount of potassium iodide and 1,4-bis-bromomethyl-benzene (1.3 g, 3.1 mmol) were added to a solution of monoalkylated compound (4-hydroxyphenyl)(4-(undec-10-en-1-yloxy)phenyl)methane (2.4 g, 6.8 mmol) in 60 mL dry N, N-Dimethylformamide (DMF). The reaction was stirred for 20 hours at 80 °C under nitrogen (N_2). The crude reaction was poured into 1 M aqueous HCl and extracted with ethyl acetate. The organic phase was washed with water, dried over $MgSO_4$, filtered and solvents were removed by evaporation under vacuum. The resulting product subjected to column chromatography (Hexane/CH_2Cl_2 1:1) to obtain the pure product (1.8 g, yield, 62.1 %) as a pale yellow solid. ^{1}H NMR (400 MHz, $CDCl_3$, ppm) δ 7.69 (s, 2H), 7.04 (d, *J* = 8.4 Hz, 4H), 7.00 (d, *J* = 8.8 Hz, 4H), 6.83 (d, *J* = 8.8 Hz, 4H), 6.74 (d, *J* = 8.4 Hz, 4H), 5.79 - 5.69 (m, 2H), 4.97 - 4.84 (m, 8H), 3.84 (t, *J* = 6.4 Hz, 4H), 3.80 (s, 4H), 2.00 - 1.94 (m, 4H), 1.72 - 1.65 (m, 4H), 1.38 -1.22 (m, 24H); ^{13}C NMR (101 MHz, $CDCl_3$, ppm) δ 157.5, 156.5, 139.2, 137.6, 134.7, 133.3, 132.3, 129.9, 129.7, 121.0, 114.9, 114.5, 114.1, 68.8, 68.0, 40.2, 33.8, 29.5, 29.4, 29.4, 29.3, 29.1, 28.9, 26.1; HRMS (ESI) m/z calc. for $C_{56}H_{69}O_4Br_2$ $[M+H]^+$: 963.3557; found 963.3572.

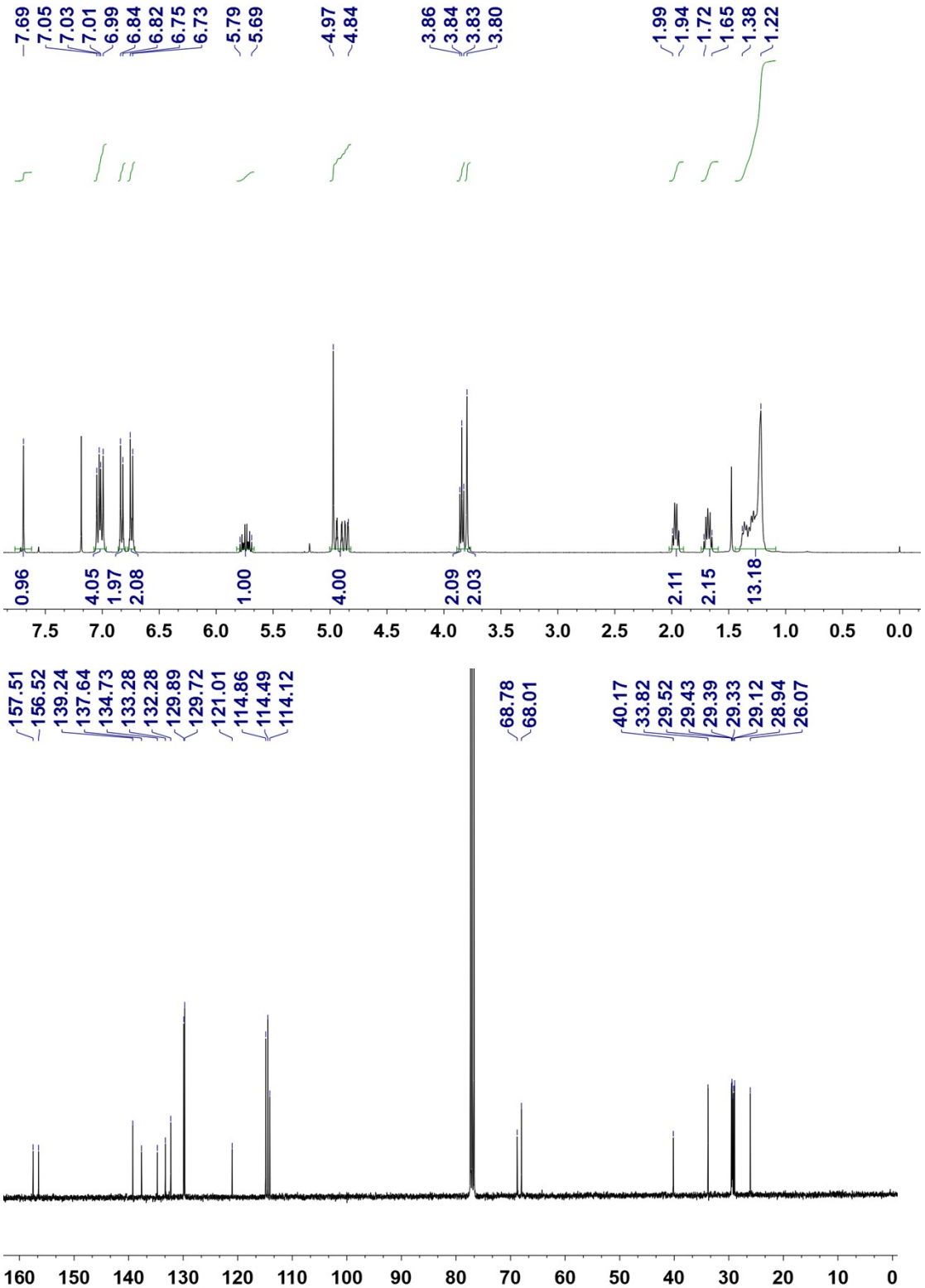
7.69
7.05
7.03
7.01
6.99
6.84
6.82
6.75
6.73
5.79
5.69
4.97
4.84
3.86
3.84
3.83
3.80
1.99
1.94
1.72
1.65
1.38
1.22
0.96
4.05
1.97
2.08
1.00
4.00
2.09
2.03
2.11
2.15
13.18
7.5
7.0
6.5
6.0
5.5
5.0
4.5
4.0
3.5
3.0
2.5
2.0
1.5
1.0
0.5
0.0
157.51
156.52
139.24
137.64
134.73
133.28
132.28
129.89
129.72
121.01
114.86
114.49
114.12
68.78
68.01
40.17
33.82
29.52
29.43
29.39
29.33
29.12
28.94
26.07
160
150
140
130
120
110
100
90
80
70
60
50
40
30
20
10
0

$N^4,N^4,N^{4''},N^{4''}$-tetraphenyl-2',5'-bis((4-(4-(undec-10-en-1-yloxy)benzyl)phenoxy)methyl)-[1,1':4',1''-terphenyl]-4,4''-diamine

4,4'-(((2,5-dibromo-1,4-phenylene)bis(methylene))bis(oxy))bis((4-(undec-10-en-1-yloxy)benzyl)benzene) (208 mg, 0.22 mmol), 4-(Diphenylamino)phenylboronic acid pinacol ester (200 mg, 0.54 mmol), Cs_2CO_3 (176 mg, 0.54 mmol), and $Pd(PPh_3)_4$ (25 mg, 0.022 mmol) were added to a mixture of toluene / ethanol / water (20 mL/ 6 / 6 mL) and bubbled with nitrogen (N_2) for 15 minutes. The reaction was stirred for 15 hours at 90 ℃ under nitrogen (N_2). The crude reaction was poured into water and extracted with ethyl acetate. The organic phase was washed with water, dried over $MgSO_4$, filtered and solvents were removed by evaporation under vacuum. The resulting product subjected to column chromatography (hexane / CH_2Cl_2 1: 1) to obtain the pure product (205 mg, 72 %) as a white solid. ^{1}H NMR (400 MHz, $CDCl_3$, ppm) δ 7.51 (s, 2H), 7.22 - 7.16 (m, 12H), 7.05 -6.93 (m, 24H), 7.74 - 6.71 (m, 8H), 5.79 -5.69 (m, 2H), 4.92 -4.84 (m, 8H), 3.83 (t, *J* = 6.8 Hz, 4H), 3.77 (s, 4H), 1.99 - 1.94 (m, 4H), 1.71 - 1.64 (m, 4H), 1.38 - 1.22 (m, 24H); ^{13}C NMR (101 MHz, $CDCl_3$, ppm) δ 157.5, 157.0, 147.6, 147.2, 140.6, 139.2, 134.1, 134.1, 133.8, 133.4, 131.2, 130.0, 129.7, 129.7, 129.3, 124.6, 123.0, 123.0, 114.9, 114.5, 114.1, 68.2, 68.0, 40.2, 33.8, 29.5, 29.4, 29.4, 29.3, 29.1, 28.9, 26.1; HRMS (ESI) m/z calc. for $C_{92}H_{97}N_2O_4$ $[M+H]^+$: 1293.7443; found 1293.7436.

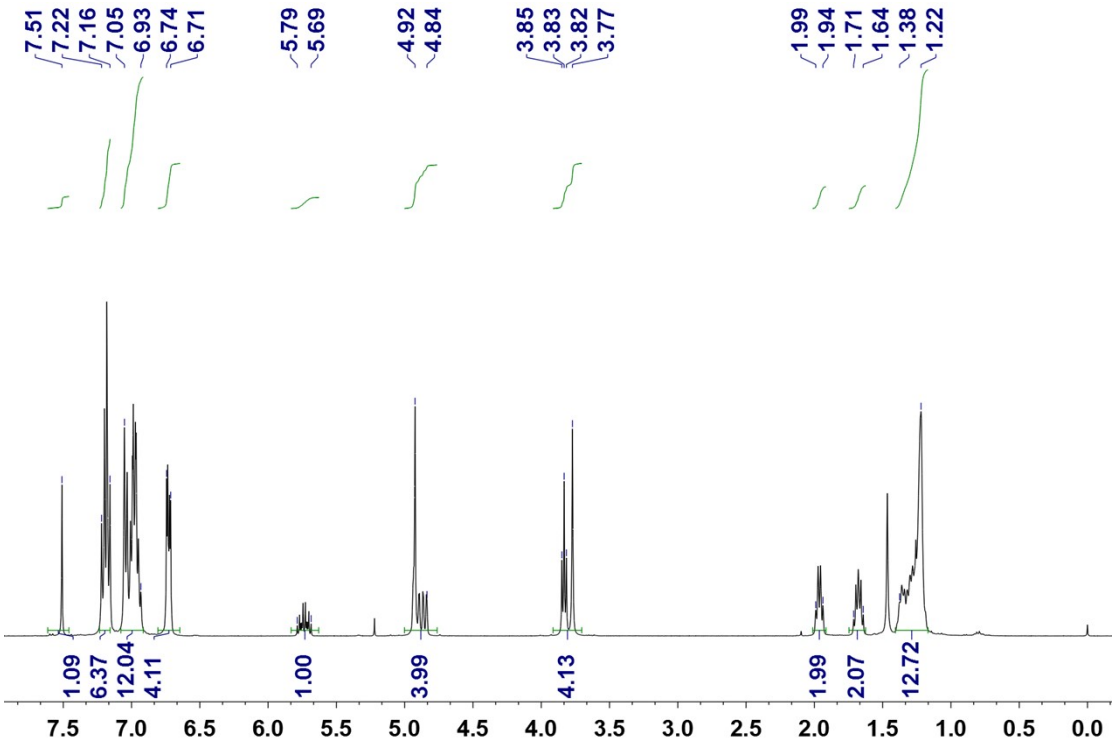

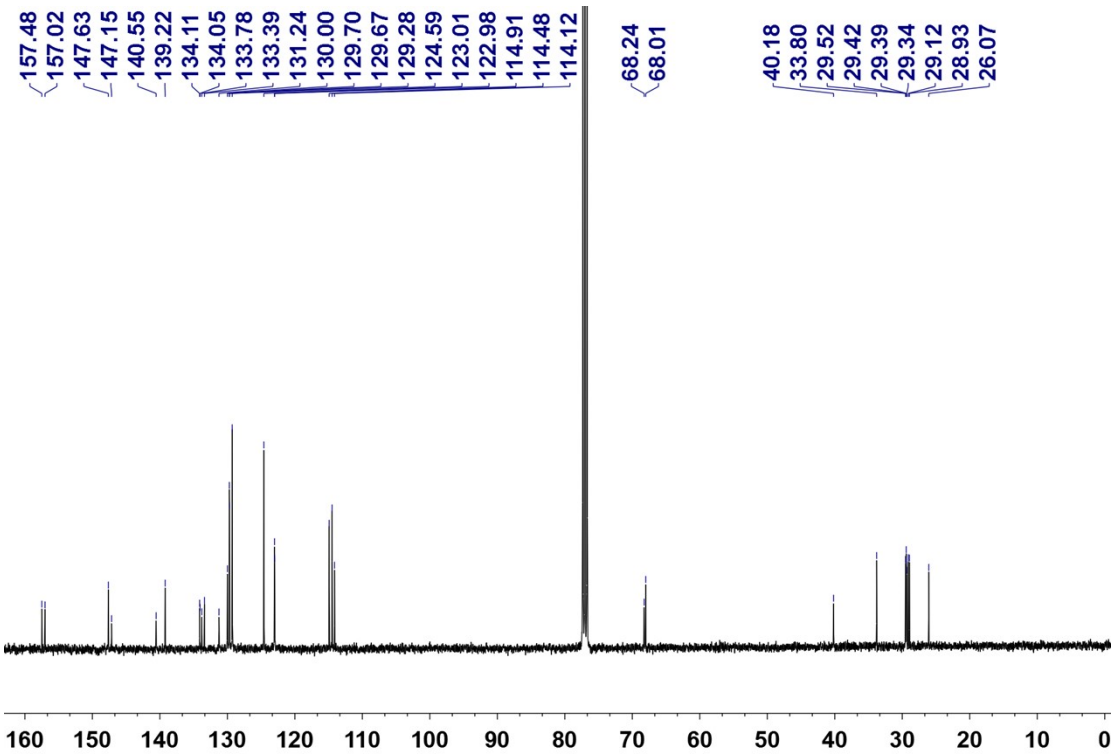

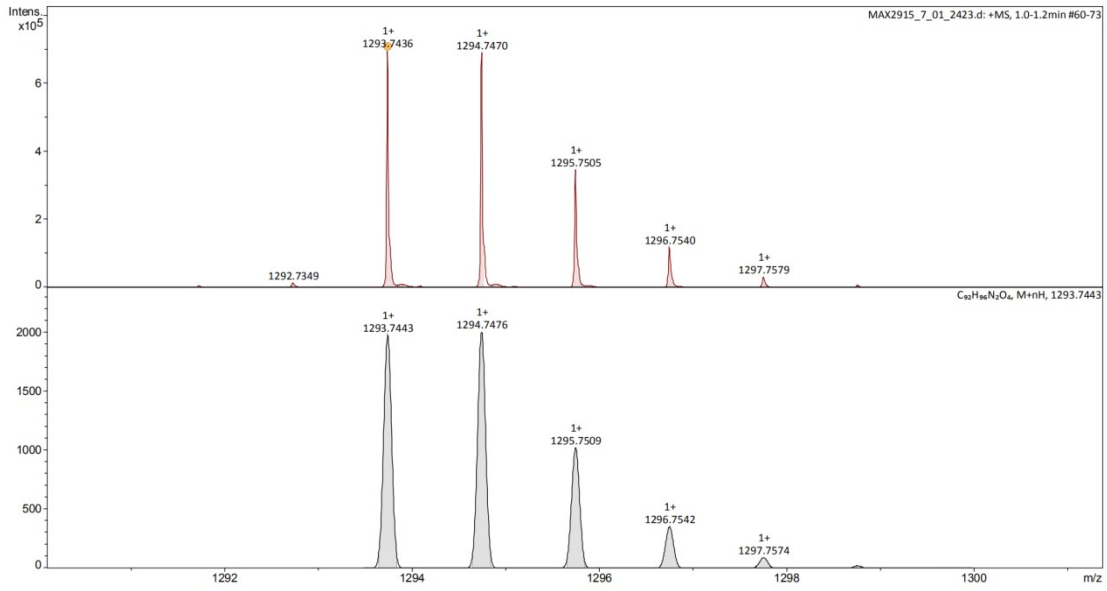

4,4'-(4,8,12,33-tetraoxa-1,3,6,9,11(1,4)-pentabenzenacyclotritriacontaphan-22-ene-62,65-diyl)bis(N,N-diphenylaniline)

Grubbs' 2nd generation catalyst (10 mg, 0.012 mmol) was added to a solution of ushape (25 mg, 0.019 mmol) in 60 mL CH_2Cl_2. The reaction was stirred was stirred under reflux overnight. The organic solvents were removed by evaporation under vacuum. The resulting product subjected to column chromatography (hexane/CH_2Cl_2 1:1) to obtain the pure product (20 mg, 82 %) as a white solid. ^{1}H NMR (400 MHz, $CDCl_3$, ppm) δ 7.51 (s, 2H), 7.28 - 7.20 (m, 12H), 7.14 - 6.99, (m, 24H), 6.78 - 6.72, (m, 8H),5.38 - 5.35 (m, 2H), 5.06 (s, 4H), 3.89 (t, J = 6.4 Hz, 4H), 3.82 (s, 4H), 2.01 - 1.95 (m, 4H), 1.77 - 1.70 (m, 4H), 1.34 - 1.27 (m, 24H); ^{13}C NMR (101 MHz, $CDCl_3$, ppm) δ 157.4, 156.7, 147.6, 147.1, 140.2, 134.2,

134.1, 133.8, 133.4, 130.5, 130.4, 130.4, 130.0, 129.7, 129.6, 129.3, 124.6, 123.0, 123.0, 115.2, 114.9, 114.5, 68.1, 67.9, 40.2, 32.5, 29.7, 29.5, 29.3, 29.3, 29.2, 29.1, 29.0, 27.2, 26.0; HRMS (ESI) m/z calc. for $C_{90}H_{93}N_2O_4$ $[M+H]^+$: 1265.7130; found 1265.7124.

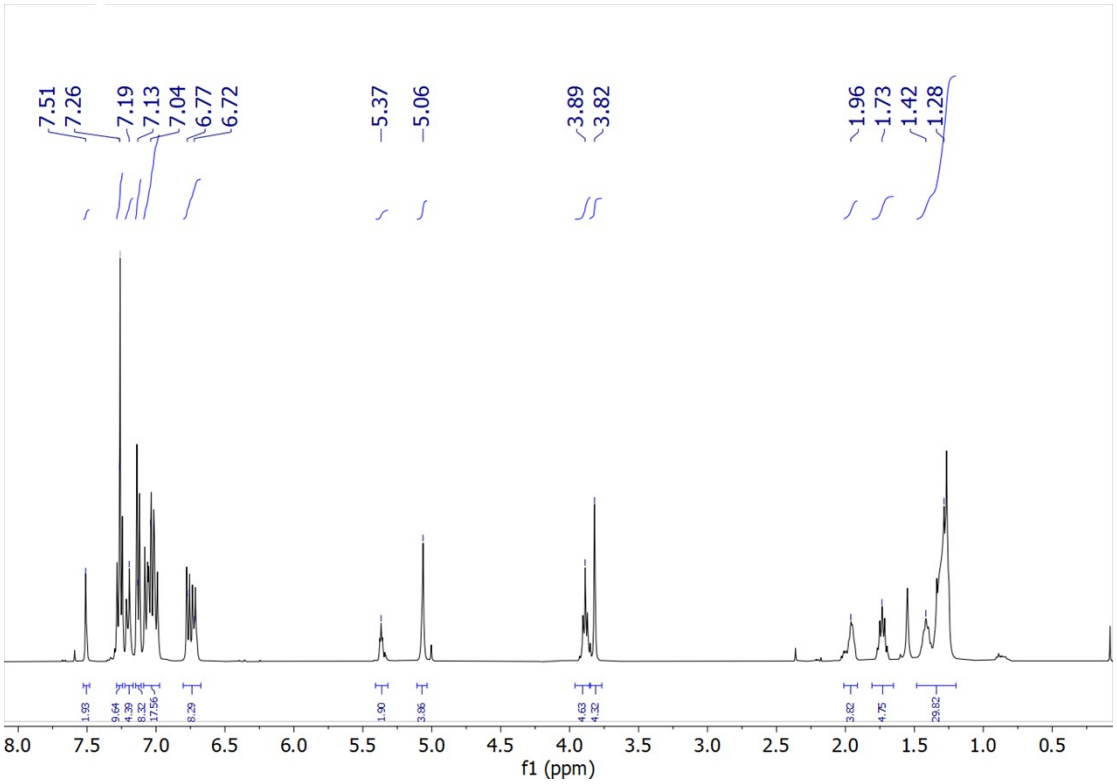

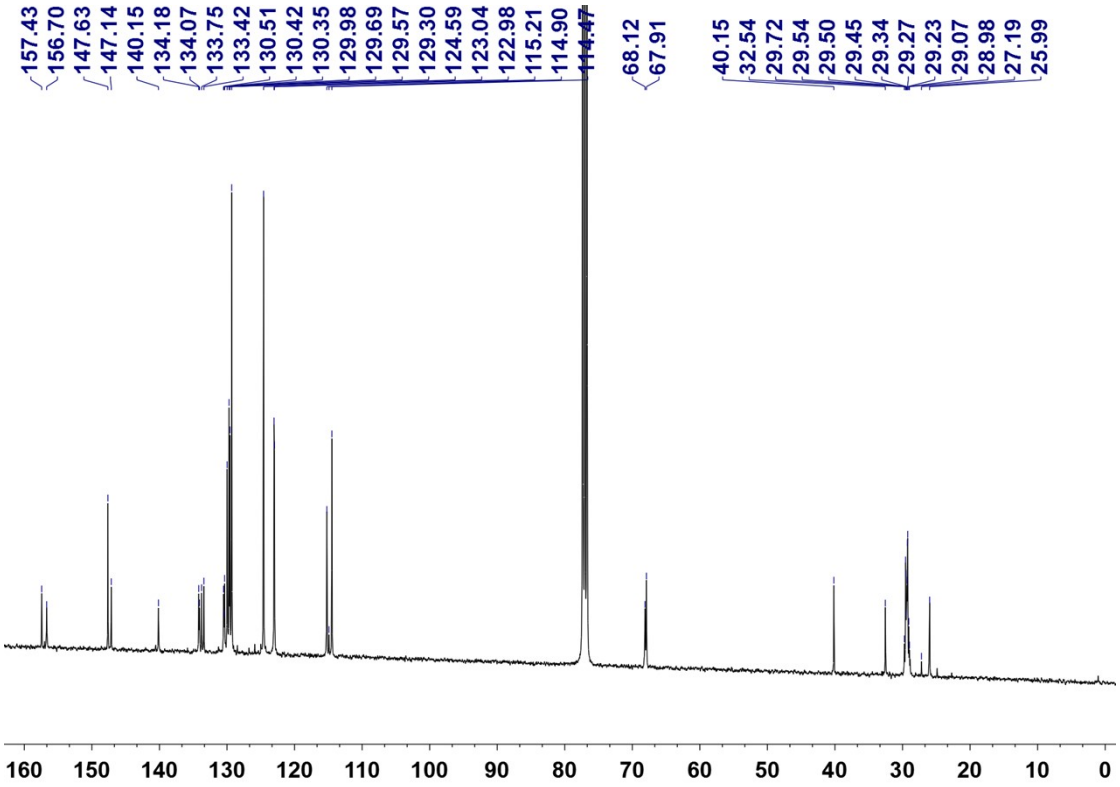

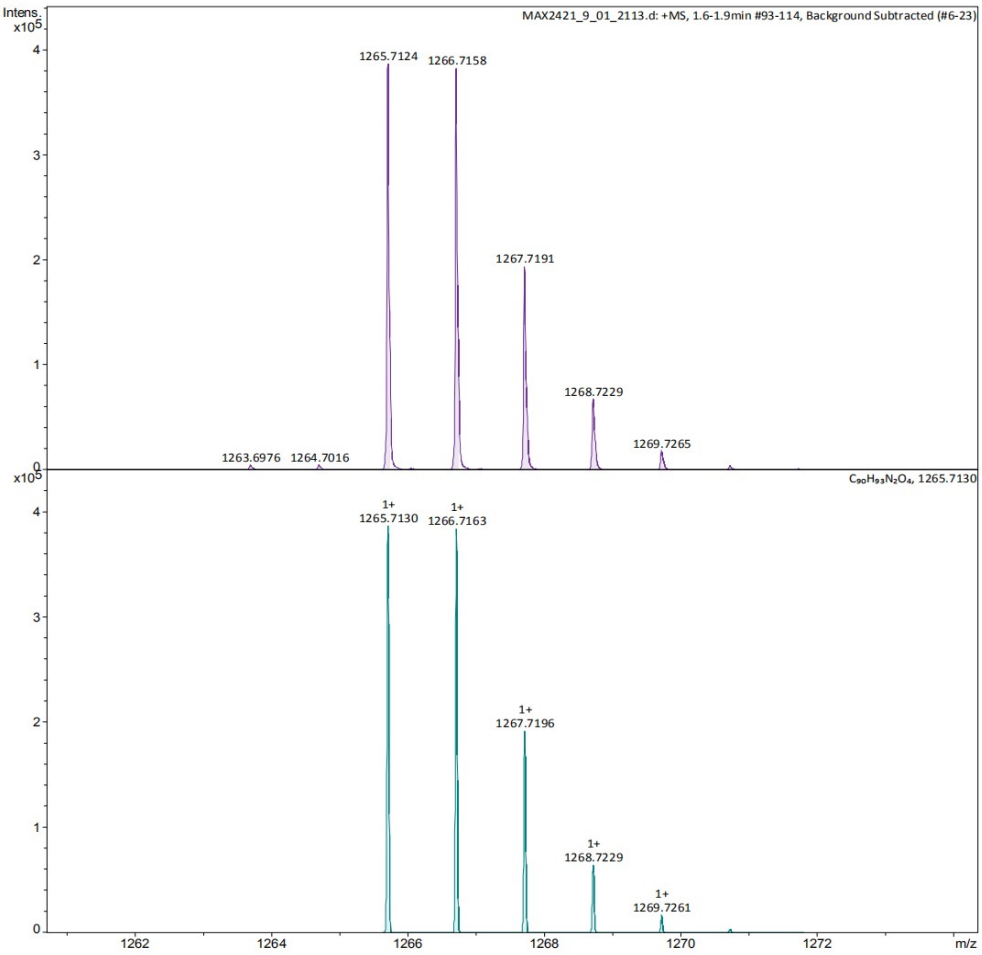

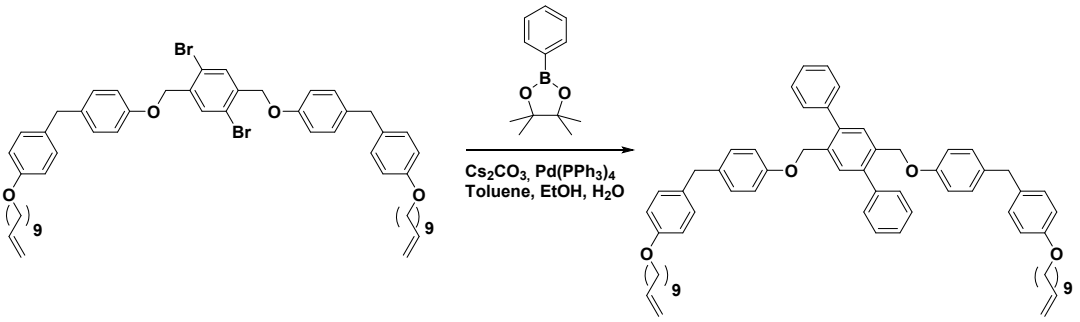

2',5'-bis((4-(4-(undec-10-en-1-yloxy)benzyl)phenoxy)methyl)-1,1':4',1''-terphenyl

4,4'-(((2,5-dibromo-1,4-phenylene)bis(methylene))bis(oxy))bis((4-(undec-10-en-1-yloxy)benzyl)benzene) (172 mg, 0.18 mmol), 4,4,5,5-tetramethyl-2-phenyl-1,3,2-dioxaborolane (167 mg, 0.45 mmol), Cs_2CO_3 (150 mg, 0.45 mmol), and $Pd(PPh_3)_4$ (21 mg, 0.018 mmol) were added to a mixture of toluene / ethanol / water (16 mL/ 5 / 5 mL) and bubbled with nitrogen (N_2) for 15 minutes. The reaction was stirred for 15 hours at 90 °C under nitrogen (N_2). The crude reaction was poured into water and extracted with ethyl acetate. The organic phase was washed with water, dried over $MgSO_4$, filtered and solvents were removed by evaporation under vacuum. The resulting product subjected to column chromatography (hexane / CH_2Cl_2 1: 1) to obtain the pure product (70 mg, 40 %) as a white solid. ^{1}H NMR (400 MHz, $CDCl_3$, ppm) δ 7.64 (s, 2H), 7.58 – 7.33 (m, 10H), 7.08 (dd, J = 8.6, 6.1 Hz, 8H), 6.95 – 6.54 (m, 8H), 5.85 (ddt, J = 16.9,

10.2, 6.6 Hz, 2H), 5.01 (m,4H), 4.98 (s, 4H), 3.94 (t, J = 6.6 Hz, 4H), 3.87 (s, 4H), 2.08 (pd, J = 6.0, 3.4 Hz, 4H), 1.88 – 1.69 (m, 4H), 1.56 – 1.30 (m, 24H); ^{13}C NMR (101 MHz, $CDCl_3$, ppm) δ 157.6, 157.1, 141.2, 140.1, 139.3, 134.2, 134.2, 133.5, 131.2, 129.8, 129.4, 128.5, 127.6, 115.0, 114.6, 114.3, 68.1, 40.3, 33.9, 29.6, 29.6, 29.5, 29.4, 29.2, 29.1, 26.2 HRMS (ESI) m/z calc. for $C_{68}H_{78}O_4$ $[M+Na]^+$: 981.5781; found 981.5781

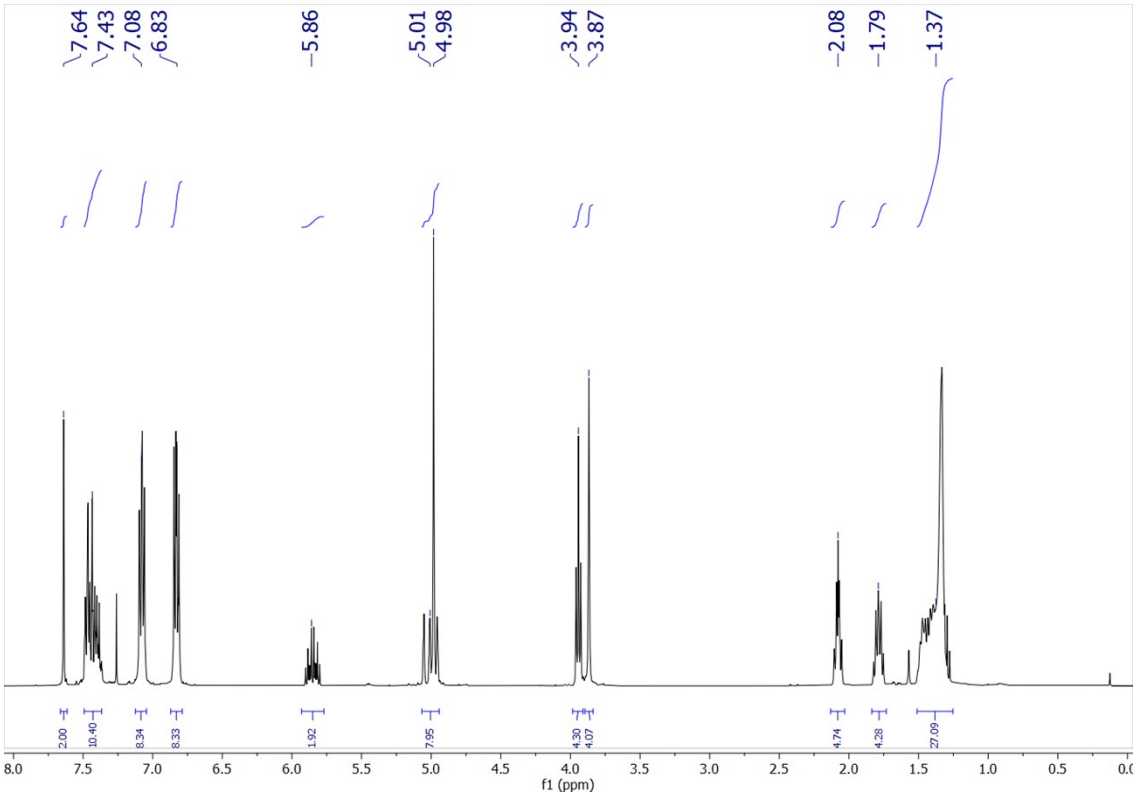

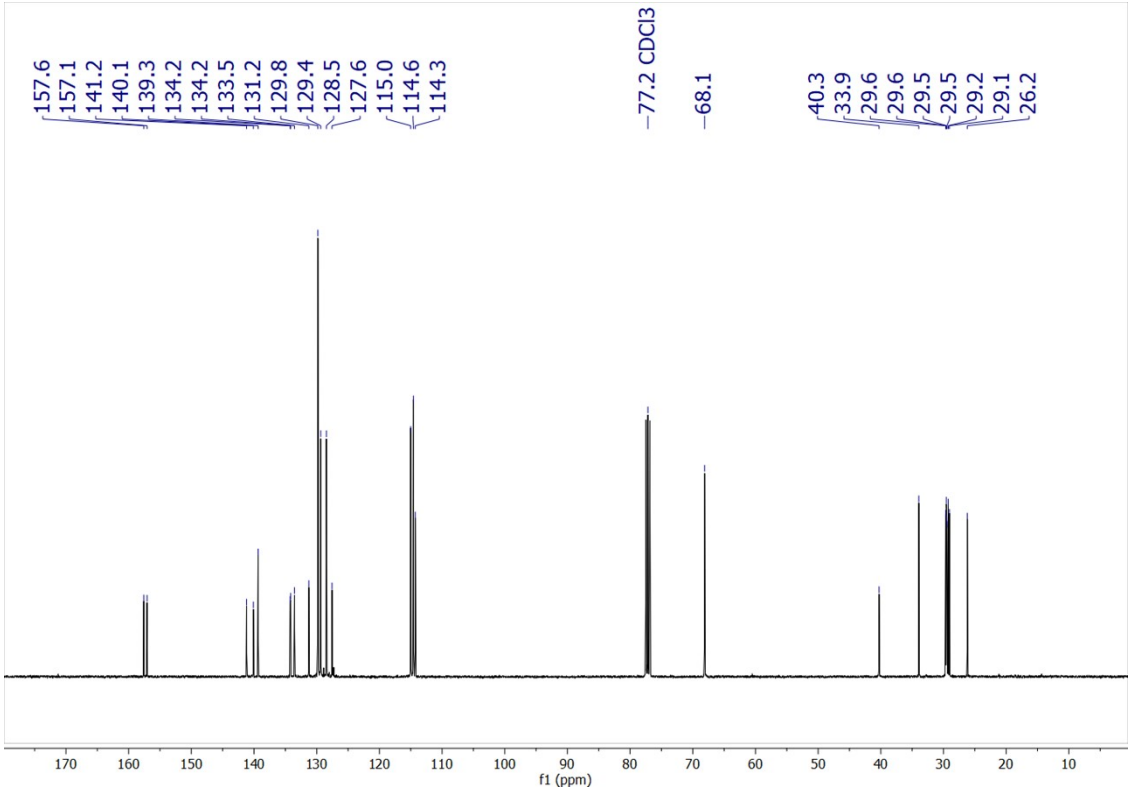

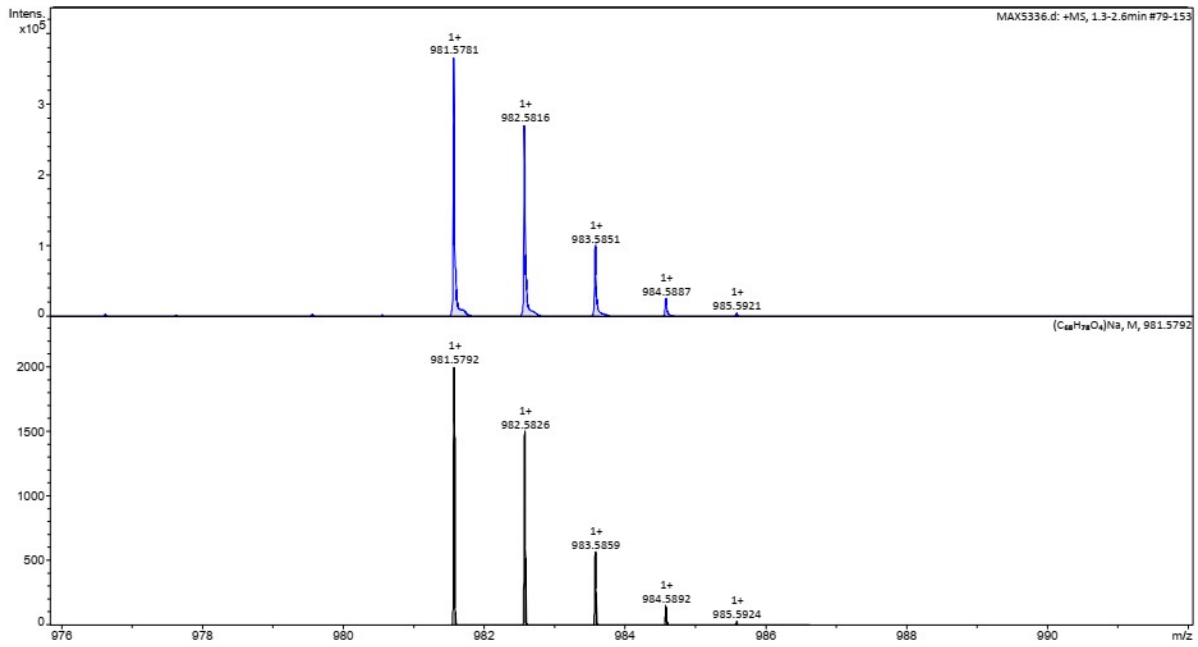

General Procedure for SWNTs Functionalization

SWNTs (20 mg) were dispersed in 20 mL of tetrachloroethane (TCE) by sonication in a bath sonicator. Subsequently, Ushape (0.01 mmol) and 2nd generation Grubbs catalyst (0.01 mmol, 17 mg) were added and the reaction was stirred at 60 °C under nitrogen for 96 hours. After this time, the suspension was filtered through a 0.2 µm pore-size polytetrafluoroethylene (PTFE) membrane and washed profusely with CH_2Cl_2 to remove any unreacted linear precursors, non-interlocked macrocycles, weakly adsorbed TPA materials, remaining catalyst, *etc*. This washing procedure was repeated three times, after which the samples were dried under vacuum and subjected to thermogravimetric analysis (TGA) to quantify the degree of functionalization.

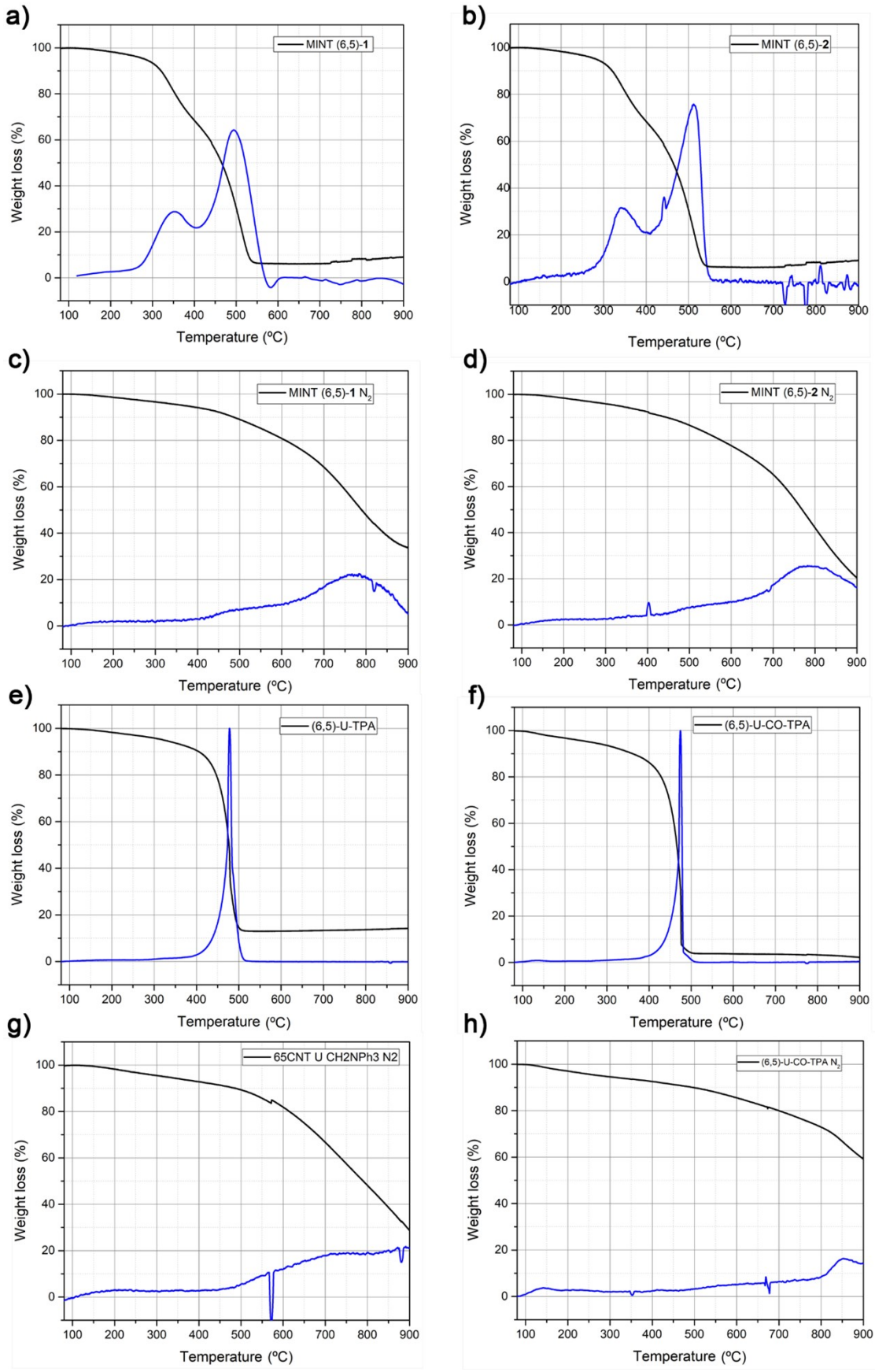

Figure S1. a-h) TGA analysis (under either air or nitrogen, 10 ºC / min) of MINT and control experiments with (6,5)-SWNTs

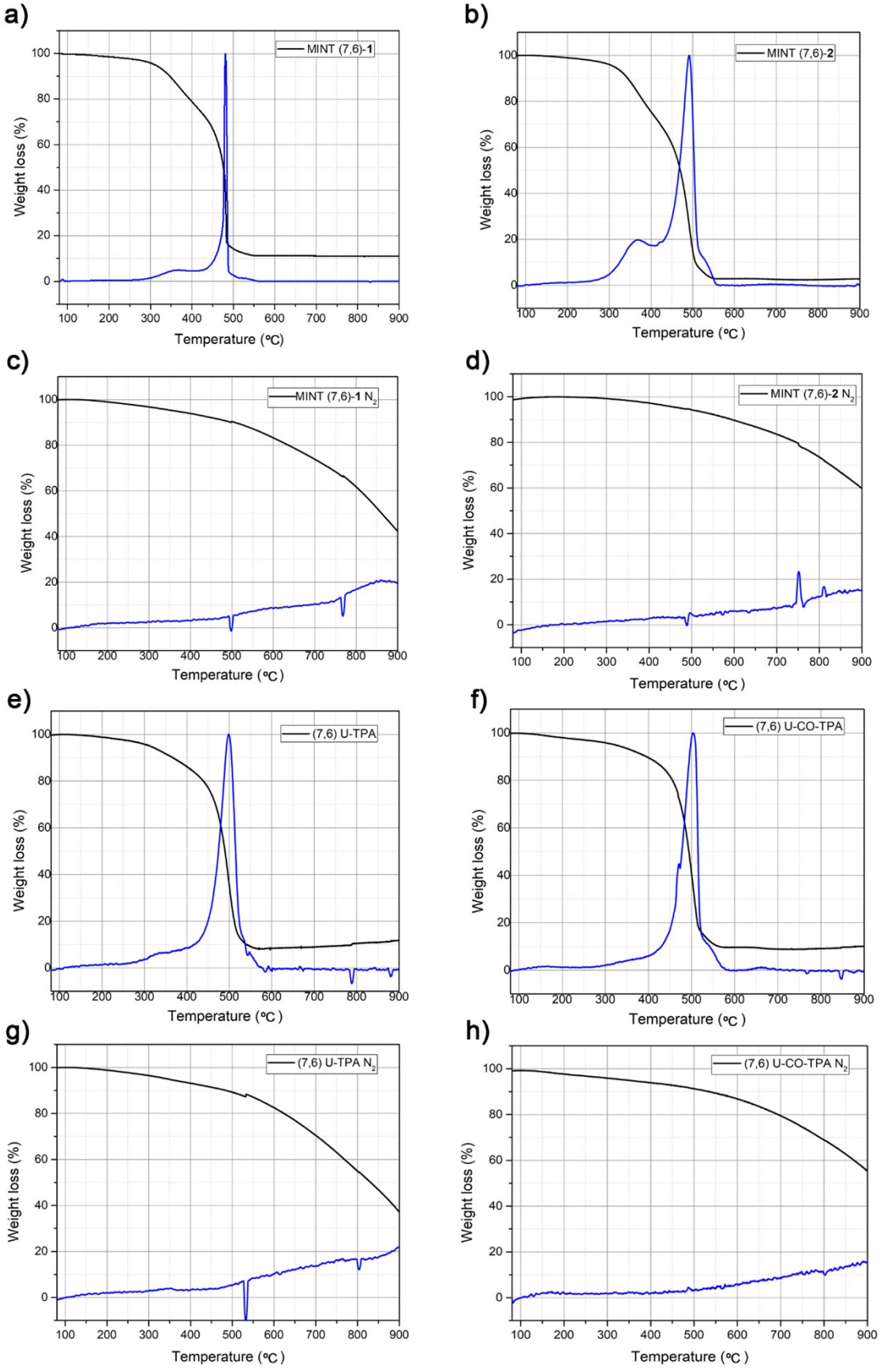

Figure S2. a-h) TGA analysis (under either air or nitrogen, 10 ºC / min) of MINT and control experiments with (7,6)-SWNTs

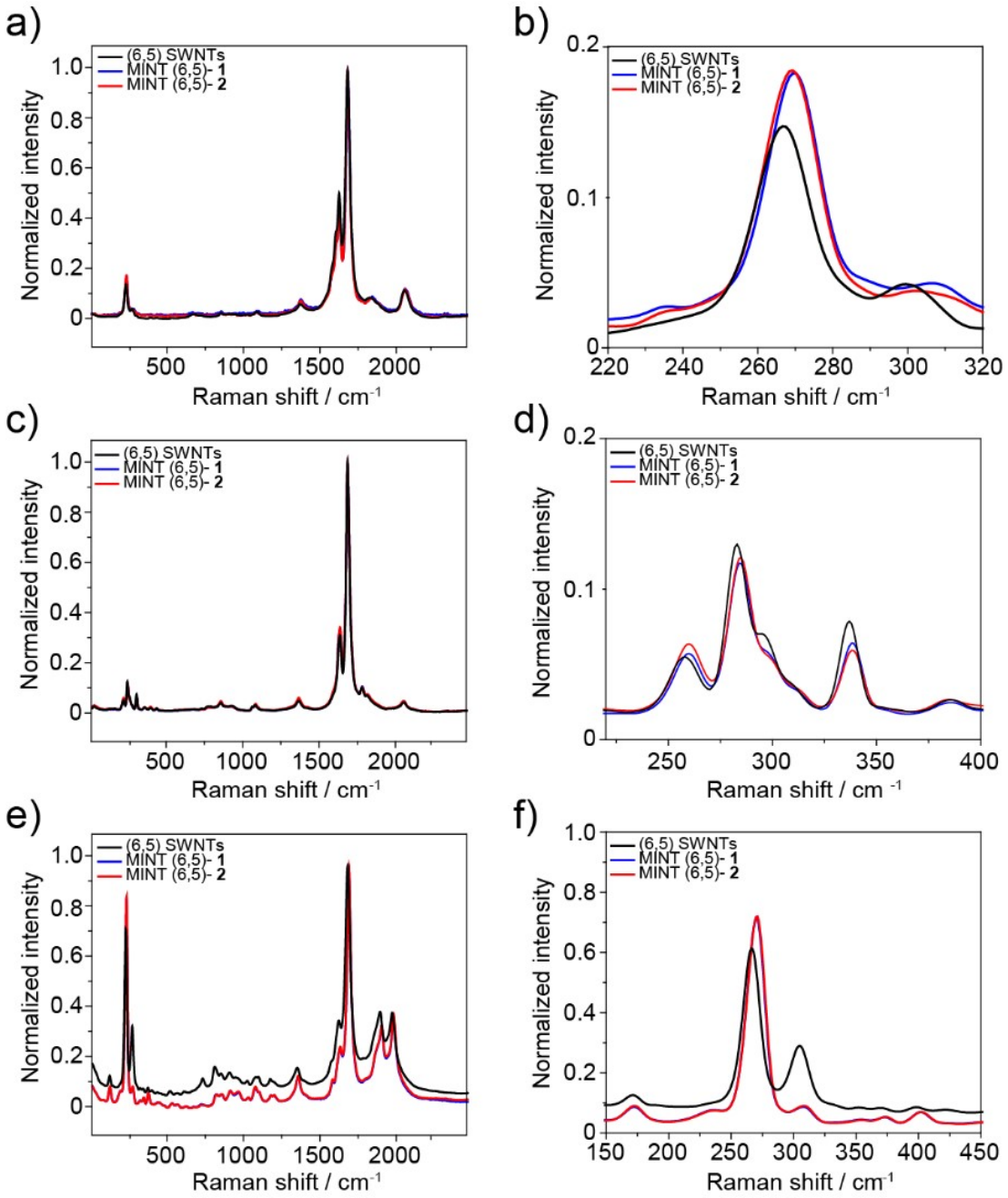

Figure S3. Raman spectra of (6,5)-SWNTs (black), MINT-(6,5)-**1** (blue) and MINT-(6,5)-**2** (red) using a) λexc=532 nm; b) magnification of the RBM zone; c) λexc=633 nm; d) magnification of the RBM zone; e) λexc=785 nm; f) magnification of the RBM zone. All spectra are the average of at least 60 different measurements.

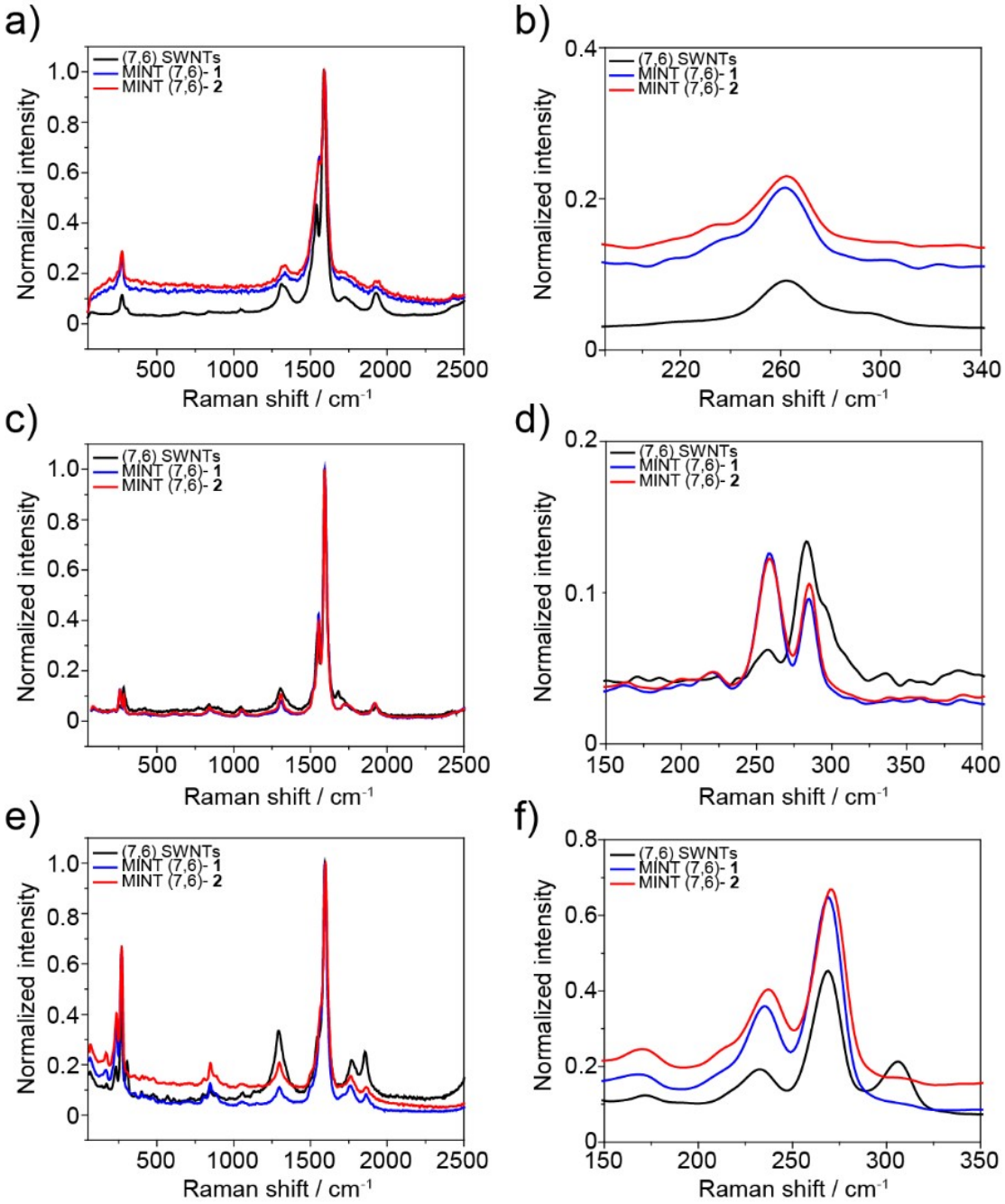

Figure S4. Raman spectra of (7,6)-SWNTs (black), MINT-(7,6)-**1** (blue) and MINT-(7,6)-**2** (red) using a) λexc=532 nm; b) magnification of the RBM zone; c) λexc=633 nm; d) magnification of the RBM zone; e) λexc=785 nm; f) magnification of the RBM zone. All spectra are the average of at least 60 different measurements.

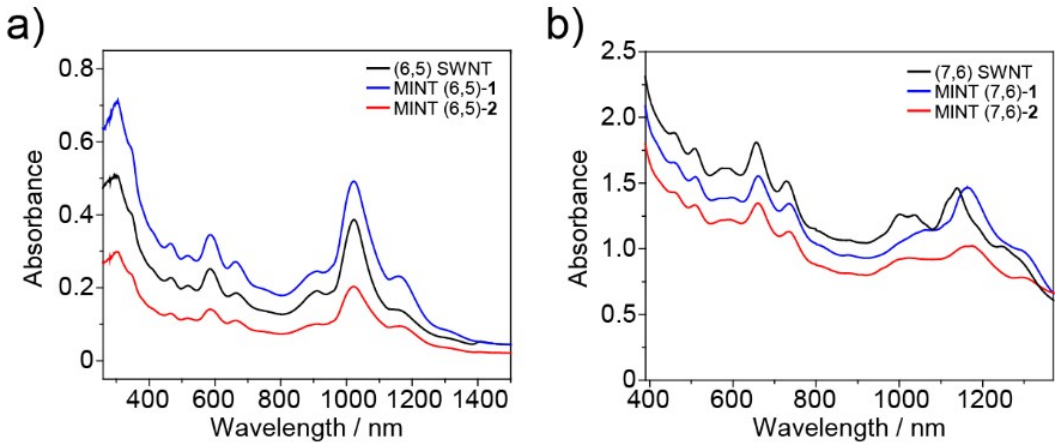

Figure S5. UV-vis-NIR (D_2O, 1% sodium dodecyl sulphate, 298 K) of a) (6,5)-SWNTs (black), MINT-(6,5)-**1** (blue), MINT-(6,5)-**2** (red); and b) (7,6)-SWNTs (black), MINT-(7,6)-**1** (blue) and MINT-(7,6)-**2** (red).

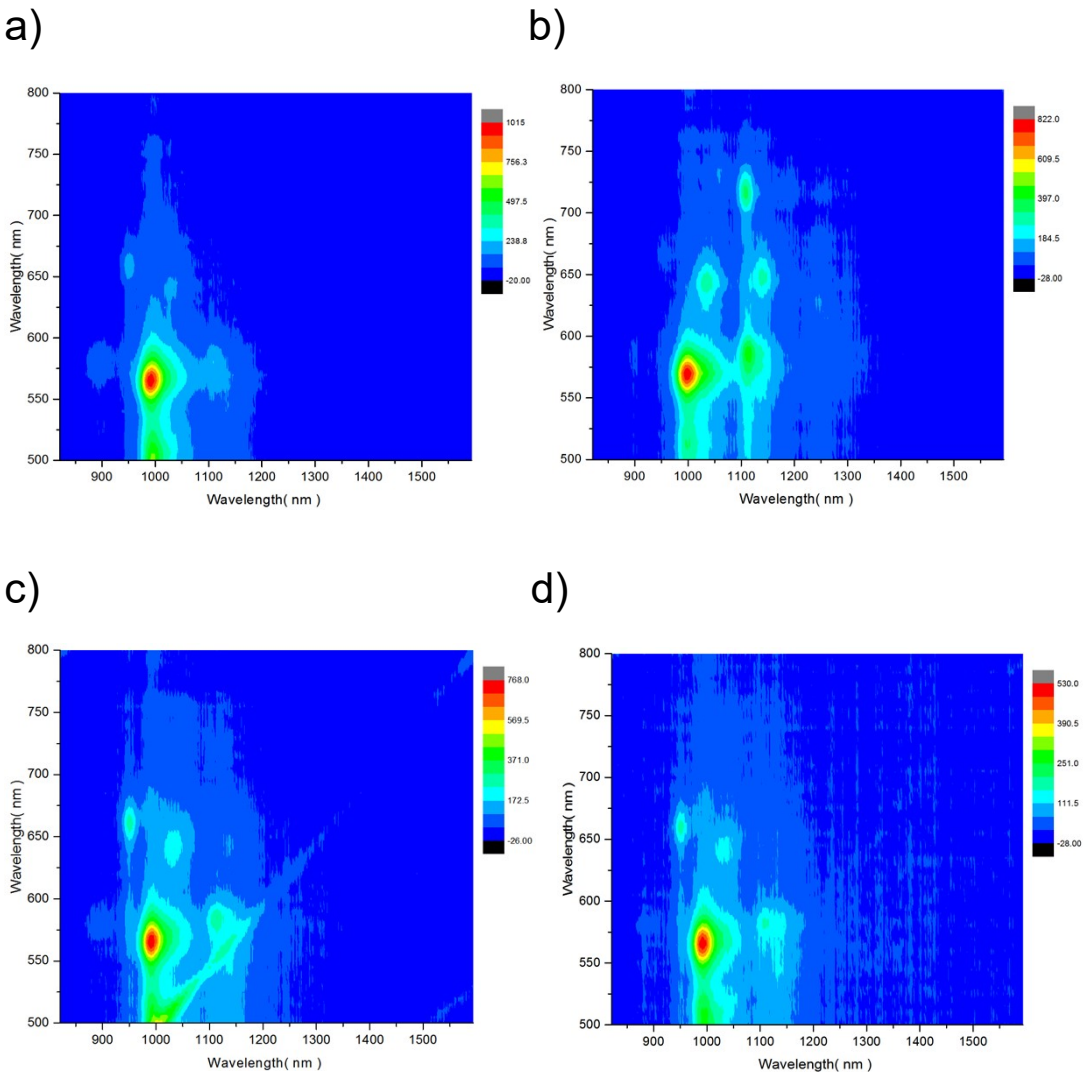

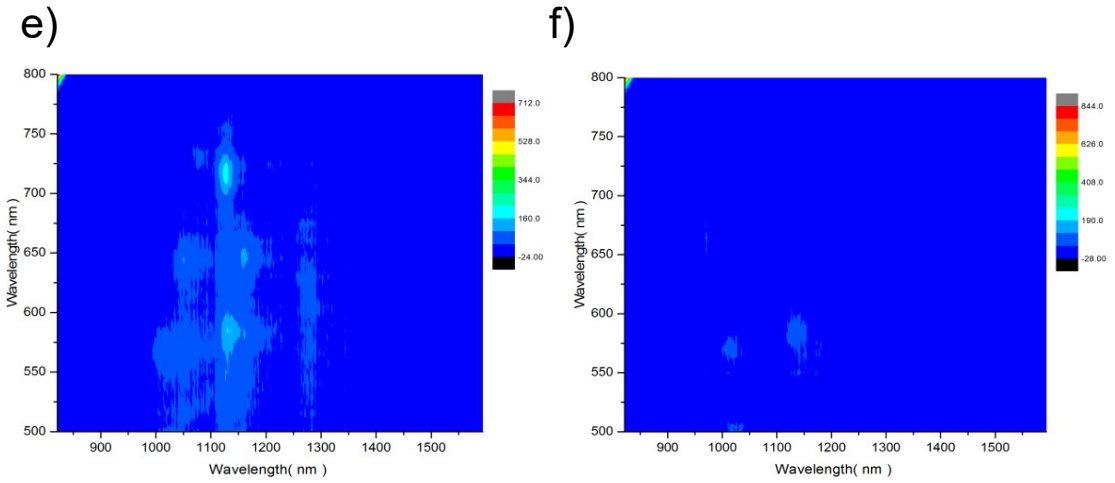

Figure S6. PLE intensity maps (D2O, 1 % SDS, 298 K) of a) (6,5)-SWNTs; b) (7,6)-SWNTs; c) MINT-(6,5)-**1**; d) MINT-(6,5)-**2**; e) MINT-(7,6)-**1**; and f) MINT-(7,6)-**2**. Rayleigh scattering has been filtered.

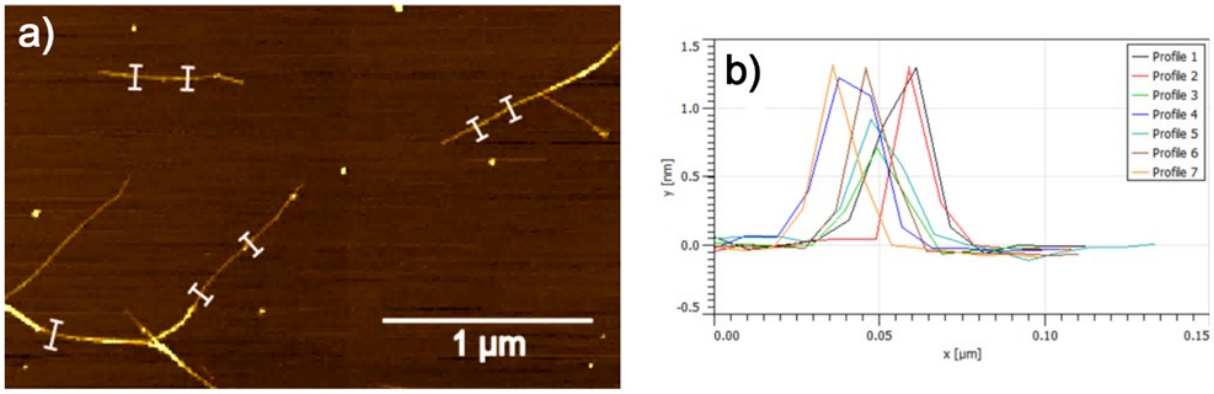

Figure S7. a) AFM topographic image of MINT (6,5)-**1**; b) Profile of selected parts on (a), showing naked SWNTs (profiles 3 and 5; Z < 1 nm), and regions with macrocyclic species (rest of profiles; Z = 1.2-1.4 nm).

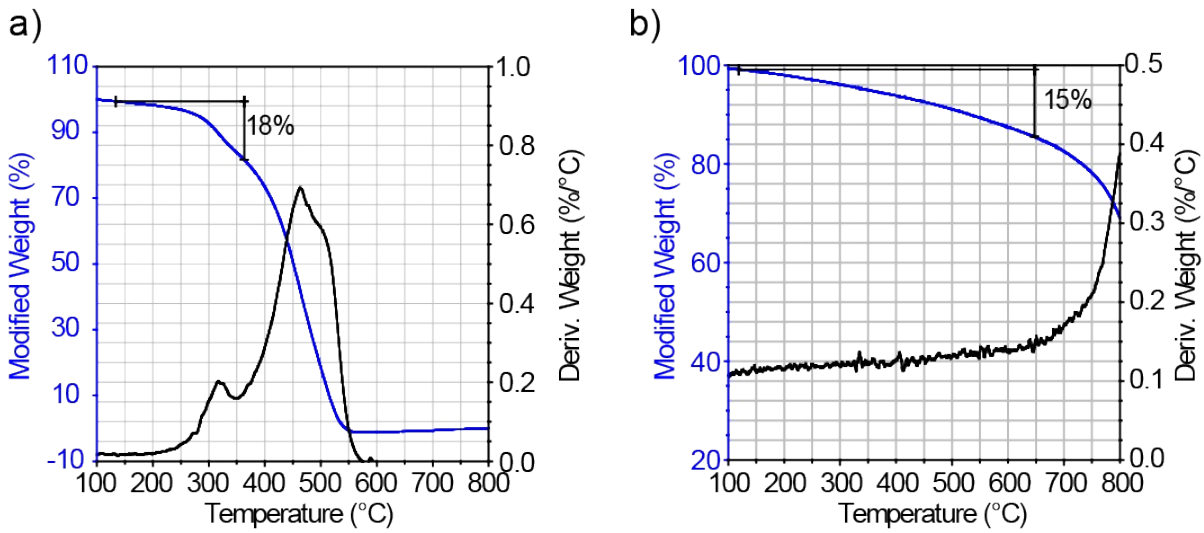

Figure S8. TGA analysis under air (a) and nitrogen (b) (10 C / min) of MINT(6,5)-**without N.**

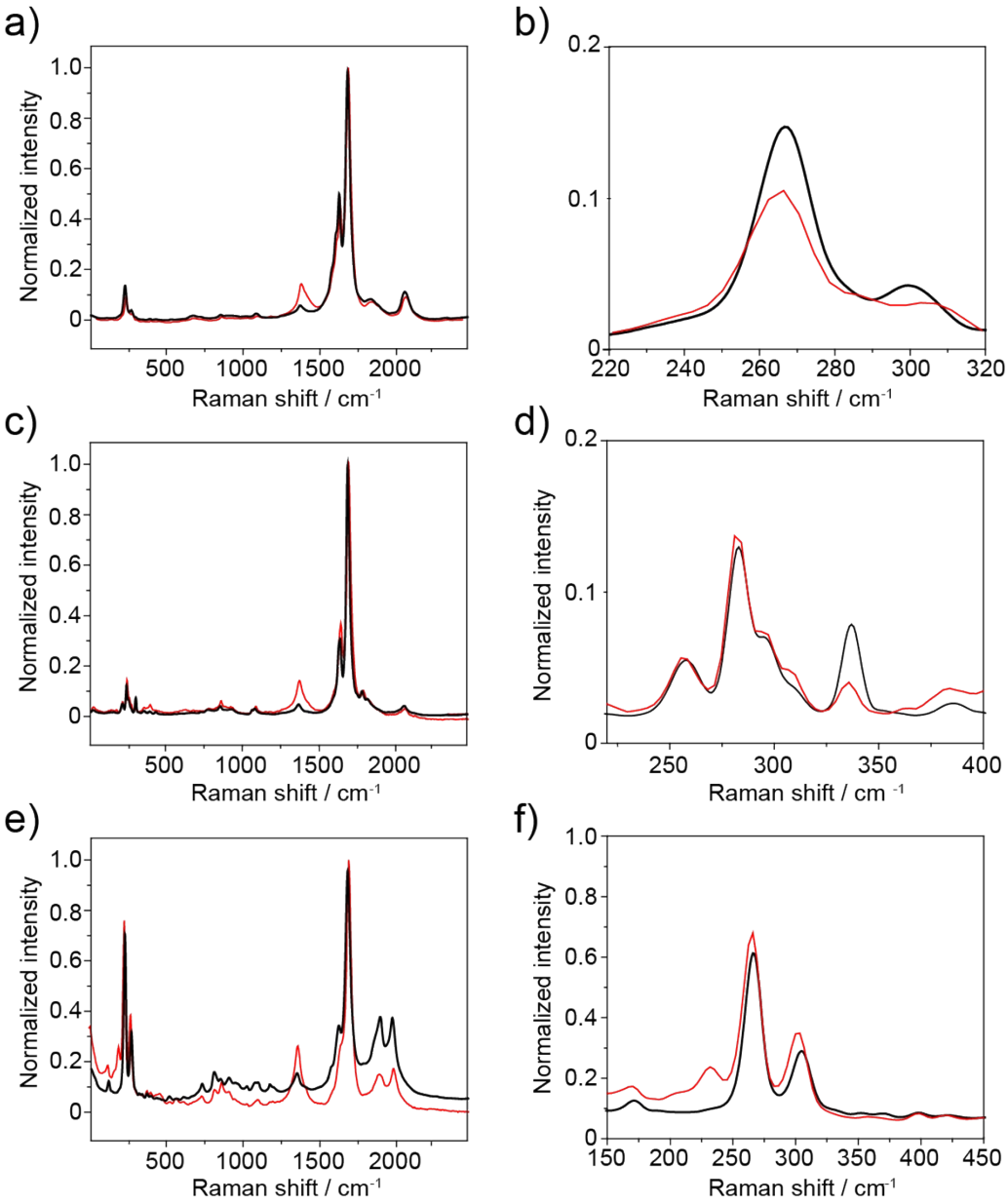

Figure S9. Raman spectra of (6,5)-SWNTs (black) and MINT-(6,5)-**without N** (red) using a) λexc=532 nm; b) magnification of the RBM zone; c) λexc=633 nm; d) magnification of the RBM zone; e) λexc=785 nm; f) magnification of the RBM zone. All spectra are the average of at least 60 different measurements.

Table S1. Raman data for MINT(6,5)-without N.

Sample	**532 nm**				**633 nm**				**785 nm**			
	I_D/I_G	Error	G	2D	I_D/I_G	Error	G	2D	I_D/I_G	Error	G	2D
(6,5)-SWNTs	0.31	0.02	1588	2627	0.23	0.03	1592	2599	0.56	0.05	1590	2576
MINT without N	0.19	0.05	1592	2615	0.16	0.05	1592	2593	0.34	0.07	1589	2570

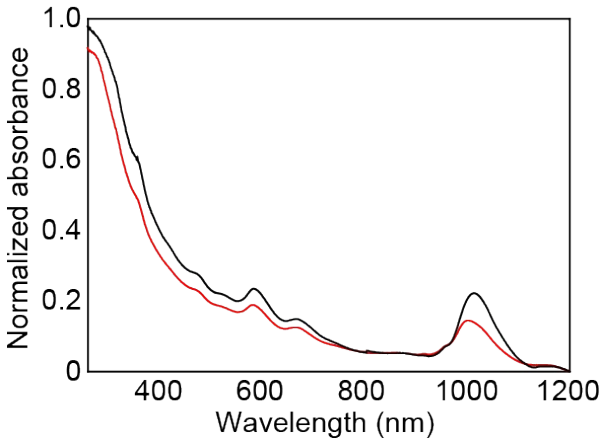

Figure S10. UV-vis-NIR (D_2O, 1% sodium dodecyl sulphate, 298 K) of (6,5)-SWNTs (black) and MINT-(6,5)-**without N** (red).

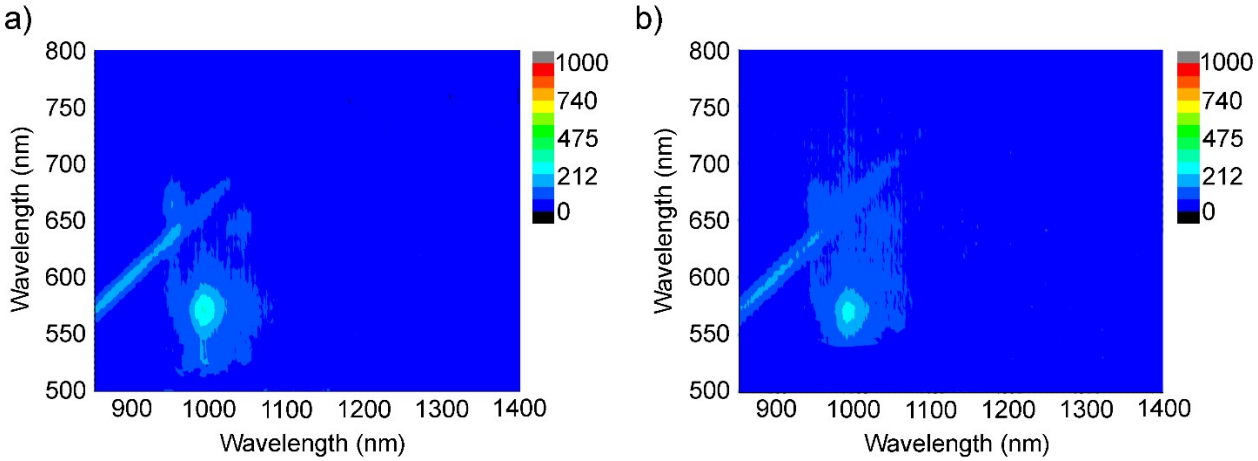

Figure S11. PLE intensity maps (D2O, 1 % SDS, 298 K) of a) (6,5)-SWNTs and b) MINT-(6,5)-**without.** Rayleigh scattering has been filtered.

Electrochemical characterization.

An Autolab potentiostat PGSTAT302N was used to measure the electrocatalytic activities towards ORR. All the electrochemical measurements were conducted in a three-electrode set-up, with a GCE, RHE and a platinum wire as working, reference and counter electrode, respectively. Rotating ring-disk electrode (RRDE) experiments were conducted in the same three-electrode system by using a 5.6 mm outer diameter glassy carbon disk tip and a Pt ring (inner diameter 6.25 mm, and outer diameter 7.92 mm). Electrochemical behavior of the macrocycles **1** (10^{-3} M) and **2** (10^{-3} M) was studied using cyclic voltammetry in a three-electrode single-compartment cell consisting of a glassy carbon working electrode, silver wire as the reference electrode, and a platinum wire as the counter electrode with ferrocene (Fc) as an internal reference. The measurements were carried out under N_2 atmosphere in anhydrous N,N-Dimethylformamide 99% using tetrabutylammonium hexafluorophosphate (0.1 M) as the supporting electrolyte. The potentials of all the reversible peaks are reported as $E_{1/2} = (Ep_a + Ep_c)/2$ in V vs Fc/Fc^+ couple.

Film electrode preparation.

To prepare the working electrode, a dispersion of 5 mg each of the samples in 1 mL of isopropanol was used as an ink. Thereafter, 20 uL of the obtained homogeneous catalyst ink was dropped onto a mirror polished glassy carbon electrode (0.196 cm^2 of geometric surface area). Subsequently, 20 uL of Nafion (5 wt%) was added and the electrode was dried under ambient conditions. The electrolyte used was 0.1 M NaOH.

Impedance measurements.

The cell resistance was measured immediately before ORR measurements taking the impedance spectra from 32 to 0.1 kHz and a voltage perturbation of 10 mV. The real part of the resistance at 1 kHz was taken as the cell resistance and was used to obtain the IR-free potential of the working electrode. All the I-E curves was corrected by the solution resistance using E= Experimental-(I*R). The used circuit model was Rs(RrCdl), including solution resistance (Rs), interfacial resistance between semiconductor electrode and electrolyte (Rr), and constant phase element (Cdl), respectively. The Nyquist plots were then fitted by Zview software using the proposed equivalent circuit model.

Electrochemical measurements.

Cyclic Voltammetry (CV) measurements under N_2 and O_2-saturated 0.1 M NaOH aqueous solution were performed to characterize the catalysts before ORR measurements. Linear Scanning Voltammetry (LSV) were conducted in an O_2-saturated 0.1 M NaOH aqueous solution to study ORR activity between 0 V and 1.0 V at a scanning rate of 5 mV s^{-1} at different rotating speed (300, 600, 900, 1200, 1600 and 2000 rpm). Stability tests were carried out by potential sweeping (0.6-1.0 V) during 5,000 ORR cycles at a rate of 100 mV/s. The electrochemical surfaces areas (ECSAs) for the catalysts

were determined from the double-layer capacitance (C_{dl}). Current densities of linear sweep voltammetry (LSV) and cyclic voltammogram (CV) were calculated from the electrode geometrical area.

Calculation of electron transferred number for ORR.

On the basis of the RDE data, the electron transfer number per oxygen molecule for oxygen reduction can be determined by Koutechy-Levich equation (1):

$$\frac{1}{J}=\frac{1}{J_L}+\frac{1}{J_K}=\frac{1}{Bw^{0.5}}+\frac{1}{J_K} \qquad (1)$$

Where J is the measured current density and w is the electrode rotating rate (rad s^{-1}). J_L and J_K are the diffusion and kinetic-limiting current densities, respectively. B is determined from the slope of the Koutechy-Levich (K-L) plot based on Levich equation (2):

$$B = 0.62nFC_o(D_o)^{2/3}v^{-1/6} \qquad (2)$$

where n is the transferred electron number, F is the Faraday constant (F = 96485 C mol^{-1}), C_0 is the O_2 concentration in the electrolyte (C_0 = 1.26 × 10-6 mol cm^{-3}), D_0 is the diffusion coefficient of O_2 (D_0 = 1.93 × 10-5 cm2 s^{-1}), and v is the kinetic viscosity (v = 0.01009cm2 s^{-1}). The constant 0.62 is adopted when the rotation speed is expressed in rad s^{-1}.

For the RRDE measurements, catalyst inks and electrodes were prepared by the same method as for RDE. The disk electrode was scanned at a rate of 5 mV s^{-1}, and the ring potential was constant at 1.2 V in 0.1 M NaOH (vs. RHE). The HO_2^-% and transfer number (n) were determined by the followed equations:[1]

$$HO_2^-\% = 200 * \frac{\frac{I_R}{N}}{I_D+\frac{I_R}{N}} \qquad (3)$$

$$n = 4 * \frac{I_D}{I_D+\frac{I_R}{N}} \qquad (4)$$

where I_d is disk current, I_R is ring current, and N is current collection efficiency of the Pt ring. N was determined to be 0.40.

Tafel slope (b) is an important parameter to determine the reaction pathway, as well as the rate determining step, which is calculated according to the Tafel equation (5) as follows:

$$\eta = a + b\log\left(\frac{j}{j_0}\right) \qquad (5)$$

When η is equal to 0, the exchange current density (j_0) can be derived from the above equation, which represents the intrinsic activity of electrocatalysts under equilibrium states.

Calculation of the Electrochemical active surface area (ECSA)

The electrochemically active surface area (ECSA) for each material was determined by the double layer capacitance (C_{dl}) and the specific capacitance (C_s) according to the following equation considering an electrode surface area ($A_{electrode}$) of 0.19625 cm^2:

$$ECSA = \frac{C_{dl}}{C_s} = \frac{slope * A_{electrode}}{C_s}$$

To obtain the C_{dl} value, CV measurements were performed in the non-Faradaic region at different scan rates (5,10, 20, 40, 60, 80, 100 and 200 mV/s) and the slope used for the equation was obtained plotting ΔJ = (Ja – Jc)/2 (at 0.2 V) against the scan rate (Figure S13), being Ja and Jc the anodic and catodic current obtained from Figure S12. The specific capacitance (C_s) of an atomically smooth planar surface with a real surface area of 1.0 cm^2 is generally within 0.02-0.06 mF/cm^2 range in alkaline media and herein as in other reported works the midpoint specific capacitance of 0.04 mF/ cm^2 was used. [2]

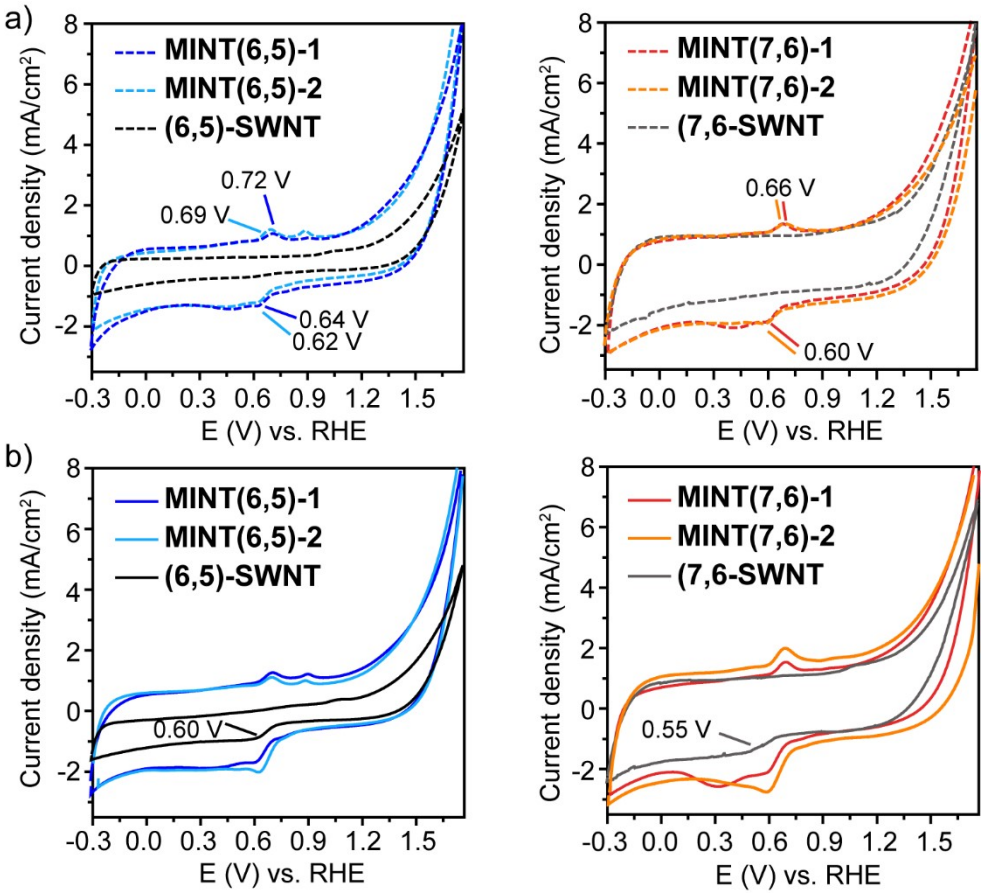

Figure S12. Cyclic voltammetry measurements for each of the obtained MINTs and the (6,5)- and (7,6)-SWNTs counterparts in a) N_2 and b) O_2-saturated 0.1 M NaOH aqueous solution with the scan rate of 50 mV s^{-1}

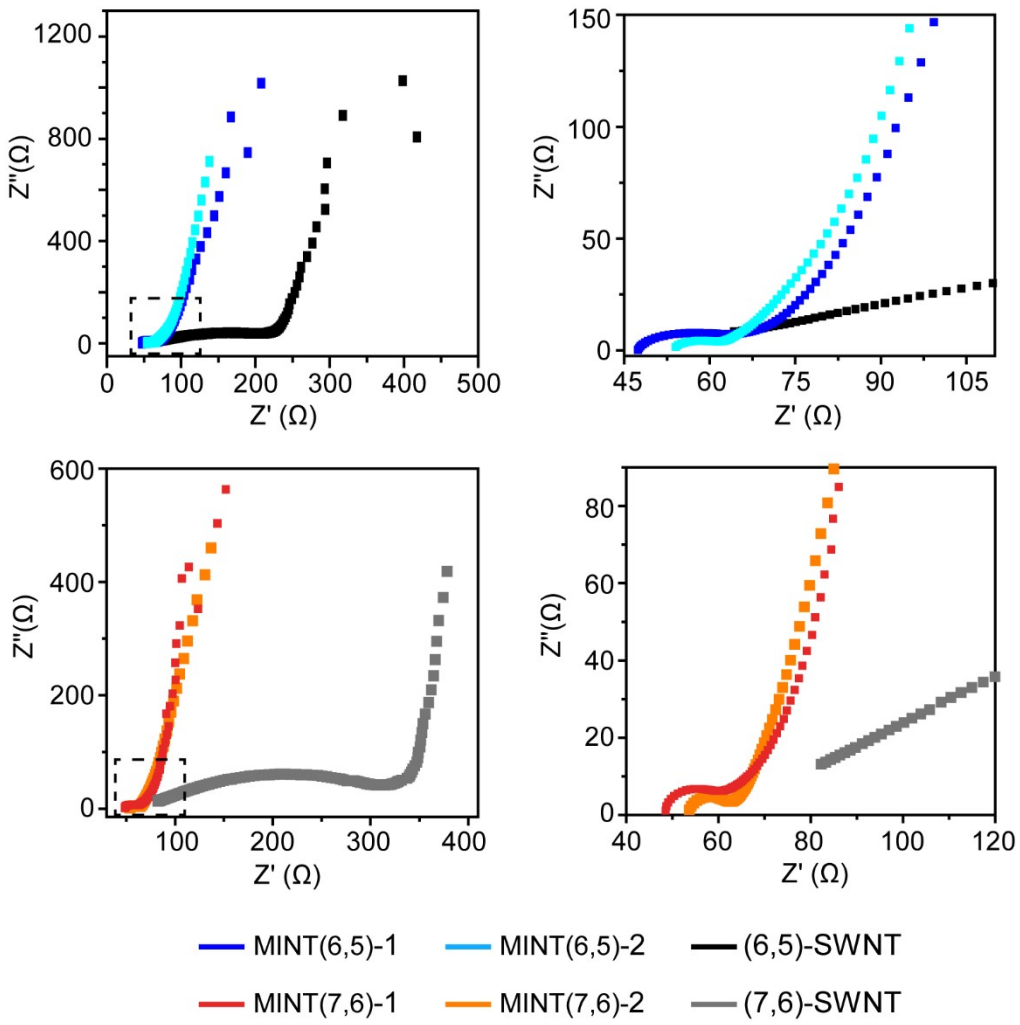

Figure S13. Electrochemical impedance spectroscopy (ESI) Nyquist plots of the different MINTs and SWNTs. The plots at the right are a zoom of the doted rectangle area of the plots at the left.

Table S2. Z-fit equivalent circuit data for the MINTs electrodes.

Catalyst	Rs (Ω)	Rr (Ω)	C_{dl} x 10^{-5} (F)
MINT(6,5)-1	48.12	16.10	1.49
MINT(6,5)-2	54.15	8.79	4.09
MINT(7,6)-1	48.56	12.05	2.68
MINT(7,6)-2	53.82	9.54	3.23
6,5-SWNT	64.30	142.87	-
7,6-SWNT	82.27	238.27	-

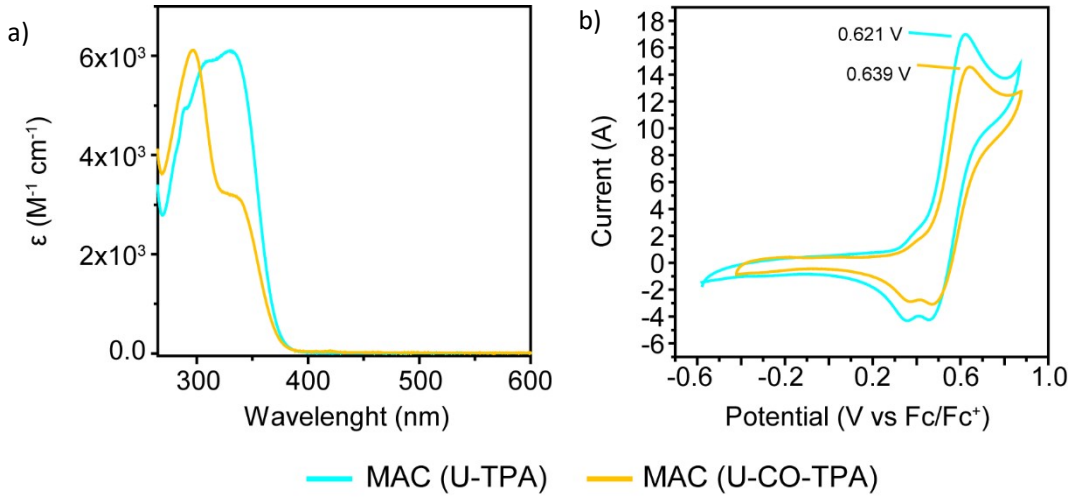

Figure S14. a) Absorption spectra in DMF and b) cyclic voltammograms in n-Bu_4NPF_6/DMF (100 mV s^{-1}) for Mac-U-TPA and Mac-U-CO-TPA both at a concentration of 10^{-5} M.

Table S3: Summary of the redox potentials and HOMO/LUMO estimated values using cyclin voltammetry (CV) and UV-vis spectra.

	Mac-U-TPA	**Mac-U-CO-TPA**
OCP (V vs Fc/Fc^+)	-0.579	-0.423
E_{OX} (V vs Fc/Fc^+)[a]	0.621	0.639
E_{HOMO} (eV) [b]	-5.420	-5.439
E_{gap} (from UV-vis) [c]	3.31	3.30
E_{LUMO} (eV) [d]	-8.731	-8.739

[a] Redox potentials from cyclic voltammetry vs. Fc/Fc^+ (0.1M Bu_4NPF_6 in DMF, scan rate 100 mV s^{-1}). [b]The highest occupied molecular orbital (HOMO) energy levels were calculated from E_{ox} values of CV diagrams and were referenced to ferrocene (4.8 eV relative to vacuum energy level). E_{HOMO} = - (4.8 + E_{ox}); [c] UV-vis absorption onset wavelengths. Optical bandgap calculated from absorption edge: E_{gap} = 1240/λ onset. [d] Lowest unoccupied molecular orbital (LUMO) energy levels was calculated from $E_{LUMO} = E_{HOMO} - E_{gap}$

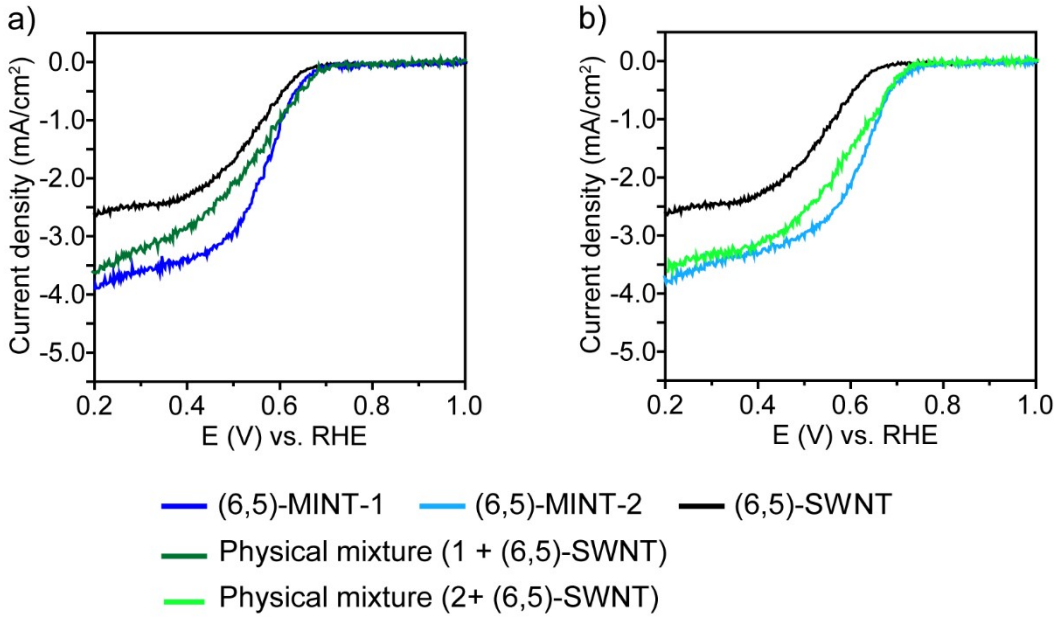

Figure S15. Comparison of the ohmic drop corrected ORR polarization curves of the physical mixtures and the MINTs electrocatalyst materials.

Table S4. ORR electro-kinetic parameter values for the physical mixture 1+ (6,5)-SWNT and 2+ (6,5)-SWNT and their respective MINTs and SWNT counterparts.

Catalyst	Half-Wave Potential ($E_{1/2}$, V *vs.* RHE)	Onset potential (E_{onset}, V *vs.* RHE)	Current density j_L at 0.2 V (mA/cm^2)	Tafel (mV/dec)	ne$^-$ (at 0.4 V *vs.* RHE)
6,5-MINT-1	0.58	0.70	3.8	111	2.3
Physical mixture (1 + (6,5)-SWNT)	**0.52**	**0.70**	**3.6**	**170**	**2.0**
6,5-MINT-2	0.62	0.74	3.7	119	2.0
Physical mixture (2 + (6,5)-SWNT)	**0.56**	**0.73**	**3.5**	**135**	**2.0**
6,5-SWNT	0.54	0.65	2.6	240	1.8

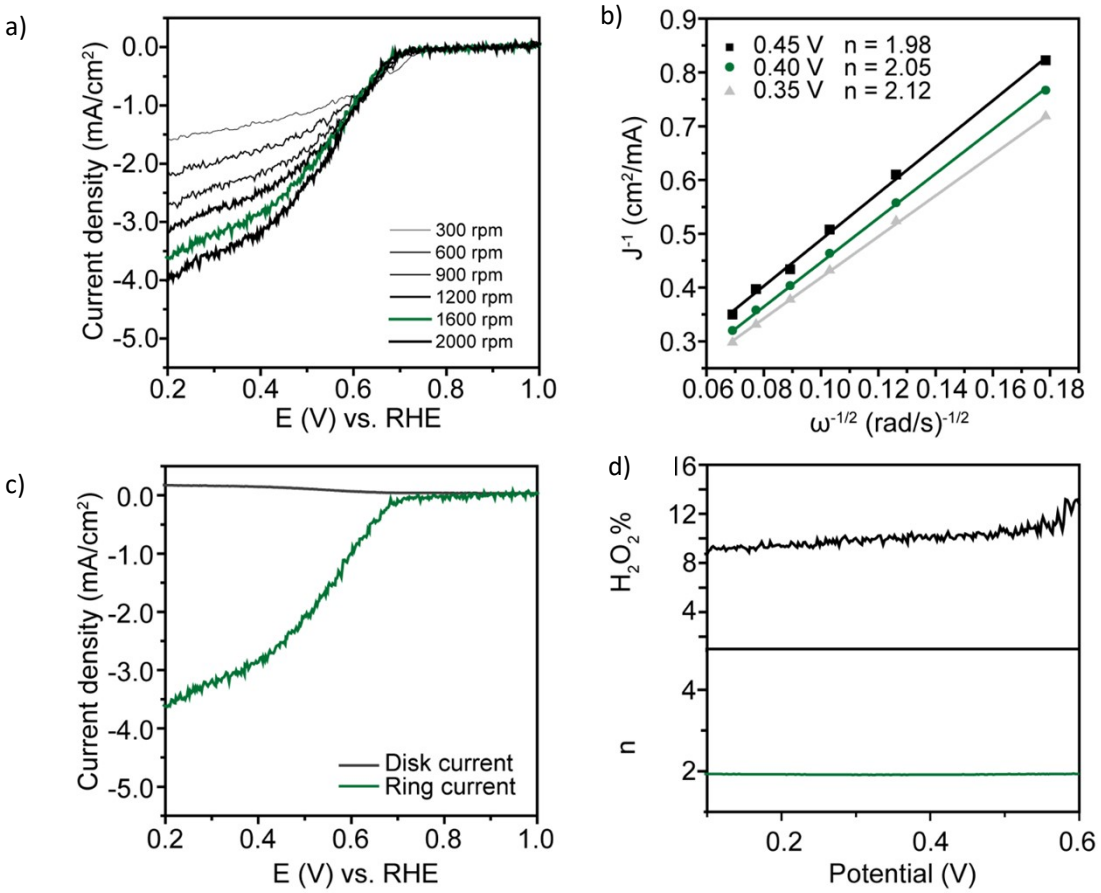

Figure S16. ORR electrochemical characterization for the **physical mixture (1 + (6,5)-SWNT)** catalyst. a) LSV curves on an RDE with various rotating speeds. b) K–L plots obtained from (a). c) RRDE voltammograms and the corresponding amperometric currents at the ring (dark line) and the disk (light line) electrodes. The electrode rotation rate was 1600 rpm, and the Pt ring electrode was 1.2 V vs. RHE. d) HO_2^- production yields and n values derived from the disk and ring currents. Measurements were performed in an O_2 saturated 0.1 M NaOH aqueous solution at the scan rate of 5 mV s^{-1}.

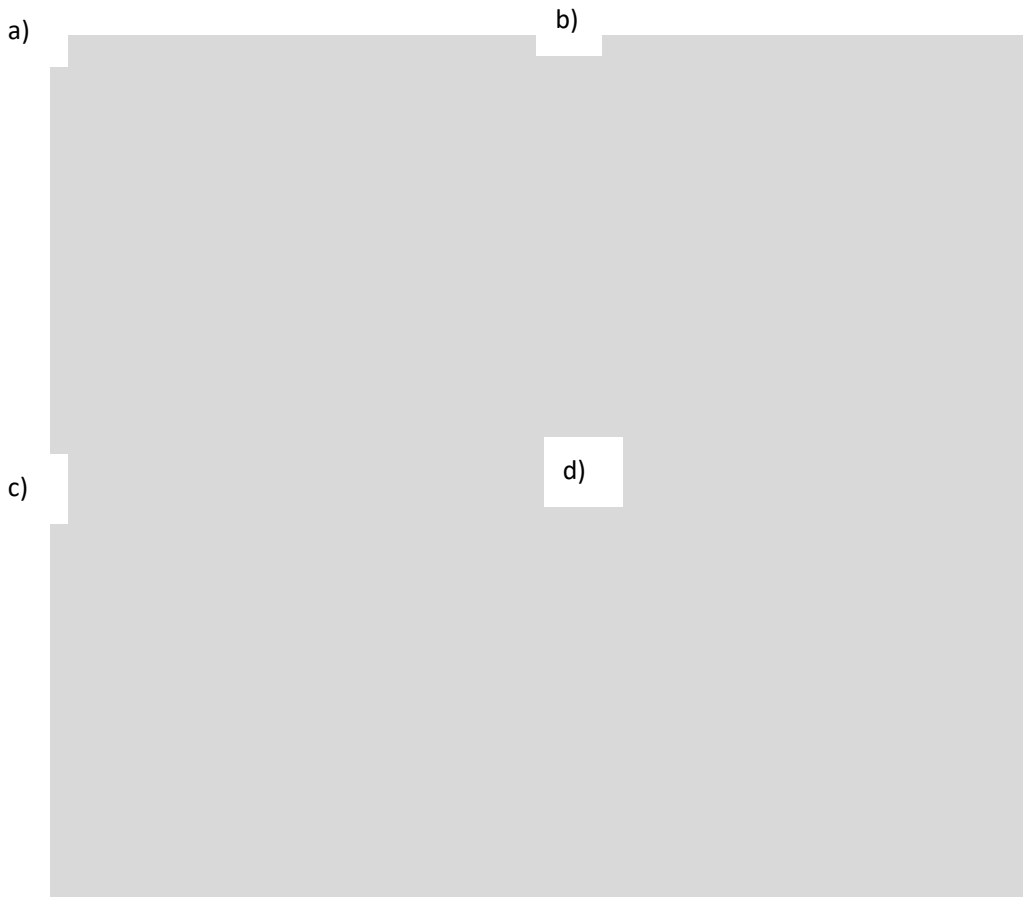

Figure S17. ORR electrochemical characterization for the **physical mixture (2 + (6,5)-SWNT)** catalyst. a) LSV curves on an RDE with various rotating speeds. b) K–L plots obtained from (a). c) RRDE voltammograms and the corresponding amperometric currents at the ring (dark line) and the disk (light line) electrodes. The electrode rotation rate was 1600 rpm, and the Pt ring electrode was 1.2 V vs. RHE. d) HO_2^- production yields and n values derived from the disk and ring currents. Measurements were performed in an O_2 saturated 0.1 M NaOH aqueous solution at the scan rate of 5 mV s^{-1}.

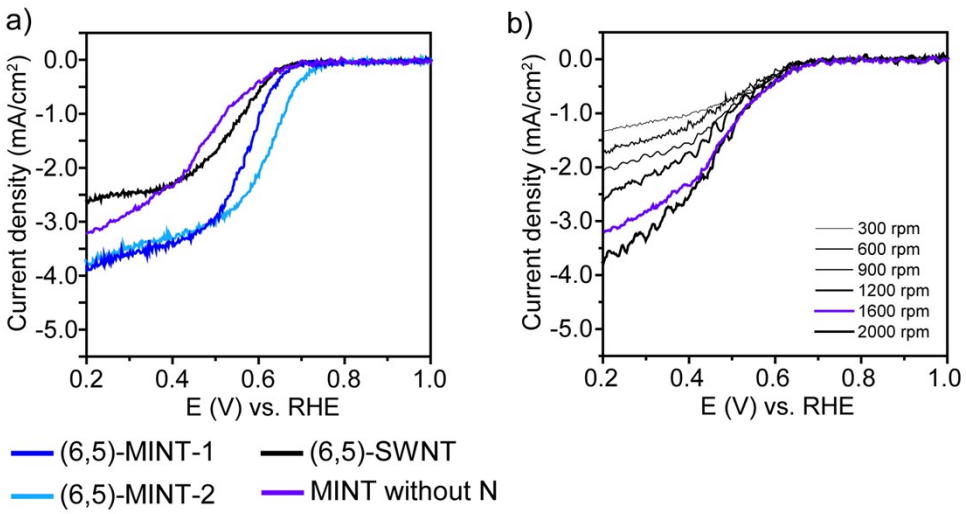

Figure S18. a) Comparison of the ohmic drop corrected ORR polarization curves of the MINT without nitrogen atoms and the respective MINTs and SWNT electrocatalyst materials. b) LSV curves on an RDE with various rotating speeds of the MINT without nitrogen electrode.

Table S5. ORR electro-kinetic parameter values for the MINT without N and their respective MINTs and SWNT counterparts.

Catalyst	Half-Wave Potential ($E_{1/2}$, V *vs.* RHE)	Onset potential (E_{onset}, V *vs.* RHE)	Current density j_L at 0.2 V (mA/cm^2)	Tafel (mV/dec)	ne$^-$ (at 0.4 V *vs.* RHE)
6,5-MINT-1	0.58	0.70	3.8	111	2.3
6,5-MINT-2	0.62	0.74	3.7	119	2.0
MINT without N	**0.46**	**0.68**	**3.2**	**250**	**1.5**
6,5-SWNT	0.54	0.65	2.6	240	1.8

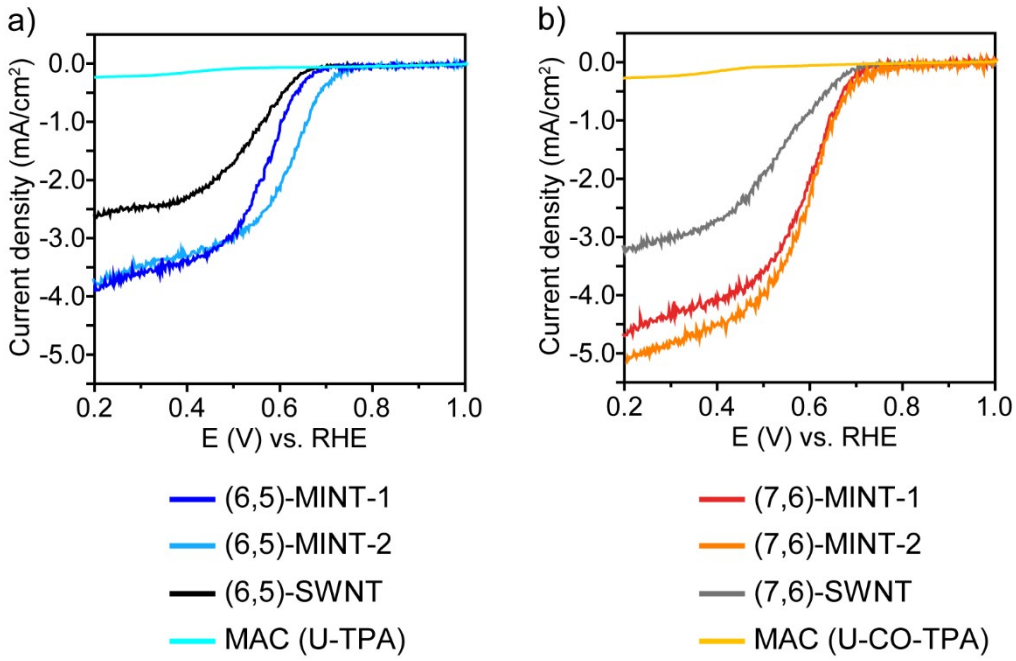

Figure S19. a) Comparison of the ohmic drop corrected ORR polarization curves of the macrocycles 1 and 2 and the MINTs and SWNT electrocatalyst materials.

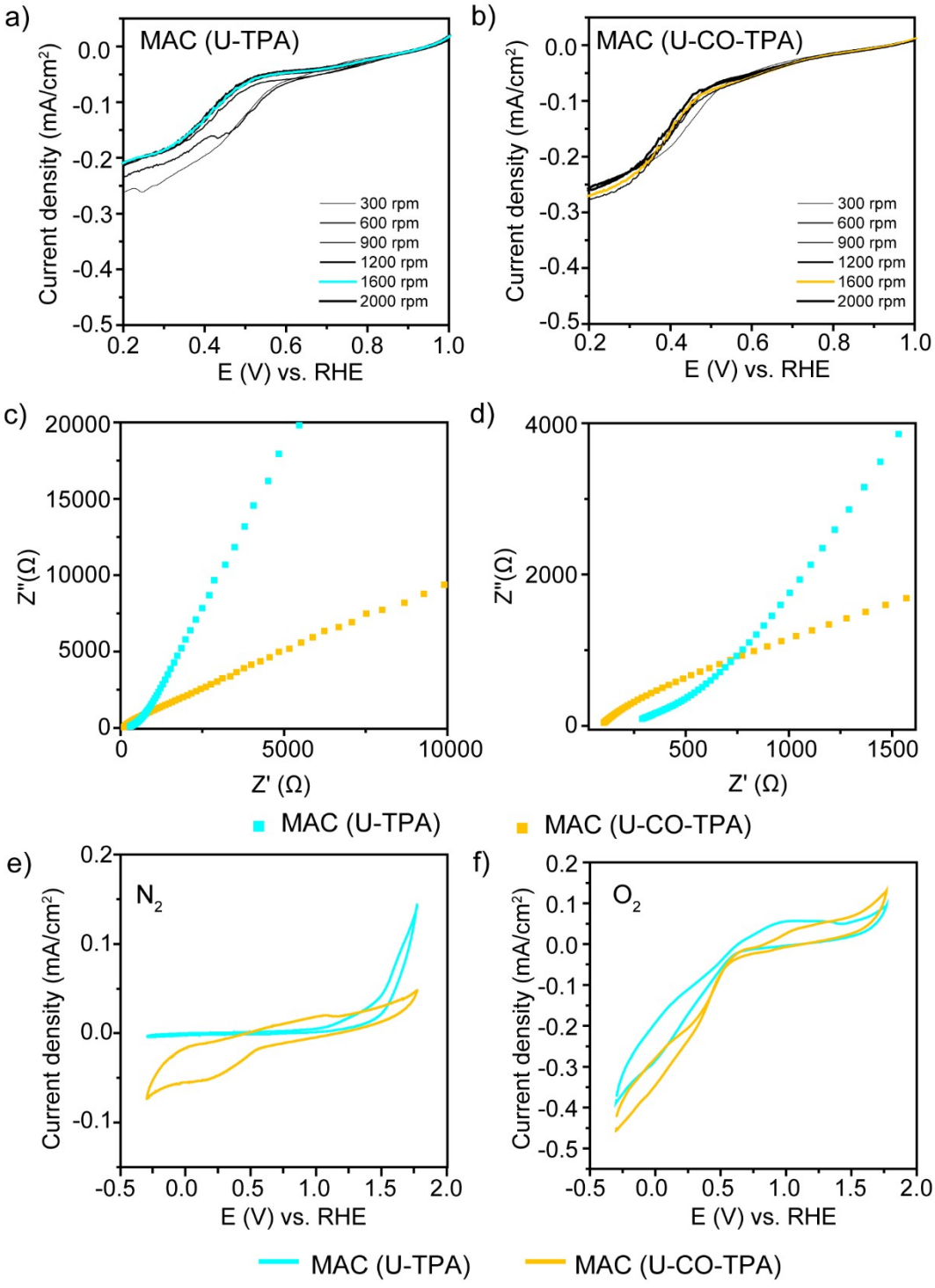

Figure S20. a-b) LSV curves on an RDE with various rotating speeds of the macrocycles, where it can be seen that the diffusion-limited current densities do not increase with increasing rotation rates. c-d) Electrochemical impedance spectroscopy (ESI) Nyquist plots of the macrocycles, showing the high resistance and e-f) Cyclic voltammetry measurements of the macrocycles immobilised on the surface of the electrode in N_2 and O_2-saturated 0.1 M NaOH aqueous solution with the scan rate of 50 mV s^{-1}.

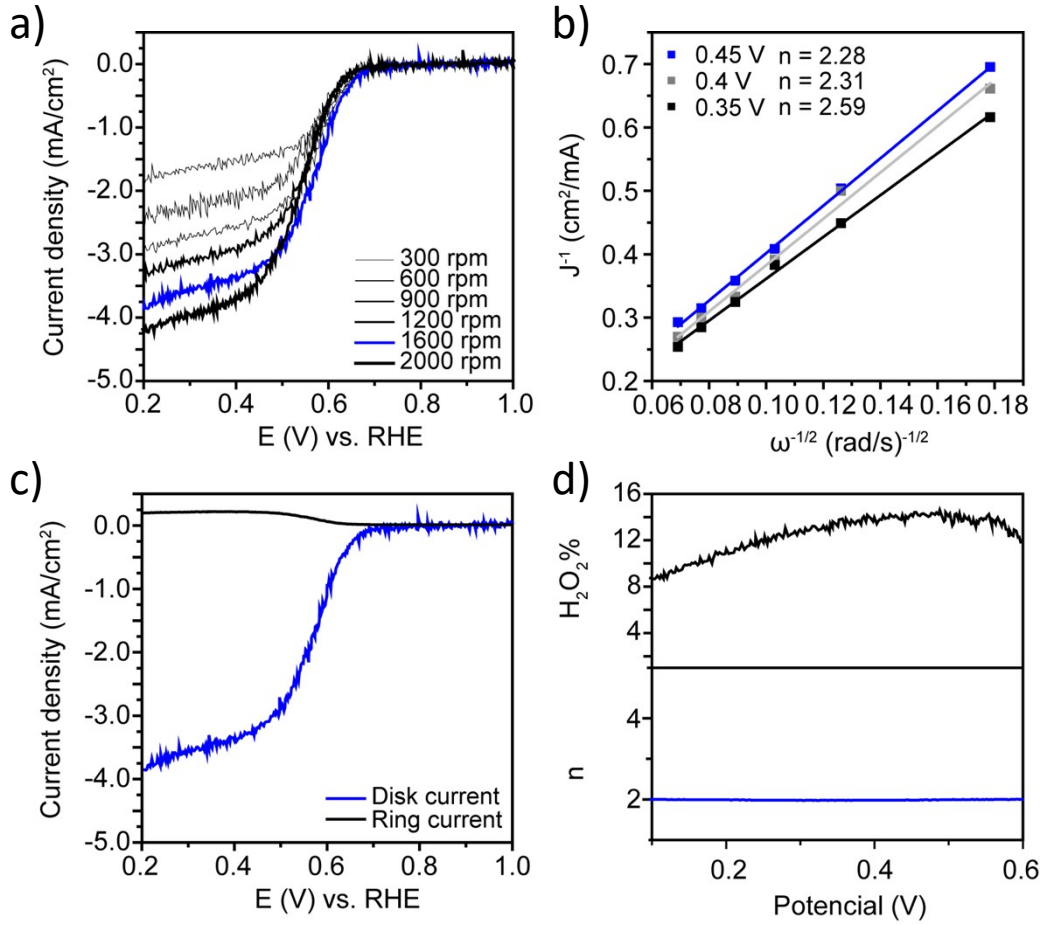

Figure S21. ORR electrochemical characterization for the MINT(6,5)-1 catalyst. a) LSV curves on an RDE with various rotating speeds. b) K–L plots obtained from (a). c) RRDE voltammograms and the corresponding amperometric currents at the ring (dark line) and the disk (light line) electrodes. The electrode rotation rate was 1600 rpm, and the Pt ring electrode was 1.2 V vs. RHE. d) HO_2^- production yields and n values derived from the disk and ring currents. Measurements were performed in an O_2 saturated 0.1 M NaOH aqueous solution at the scan rate of 5 mV s^{-1}.

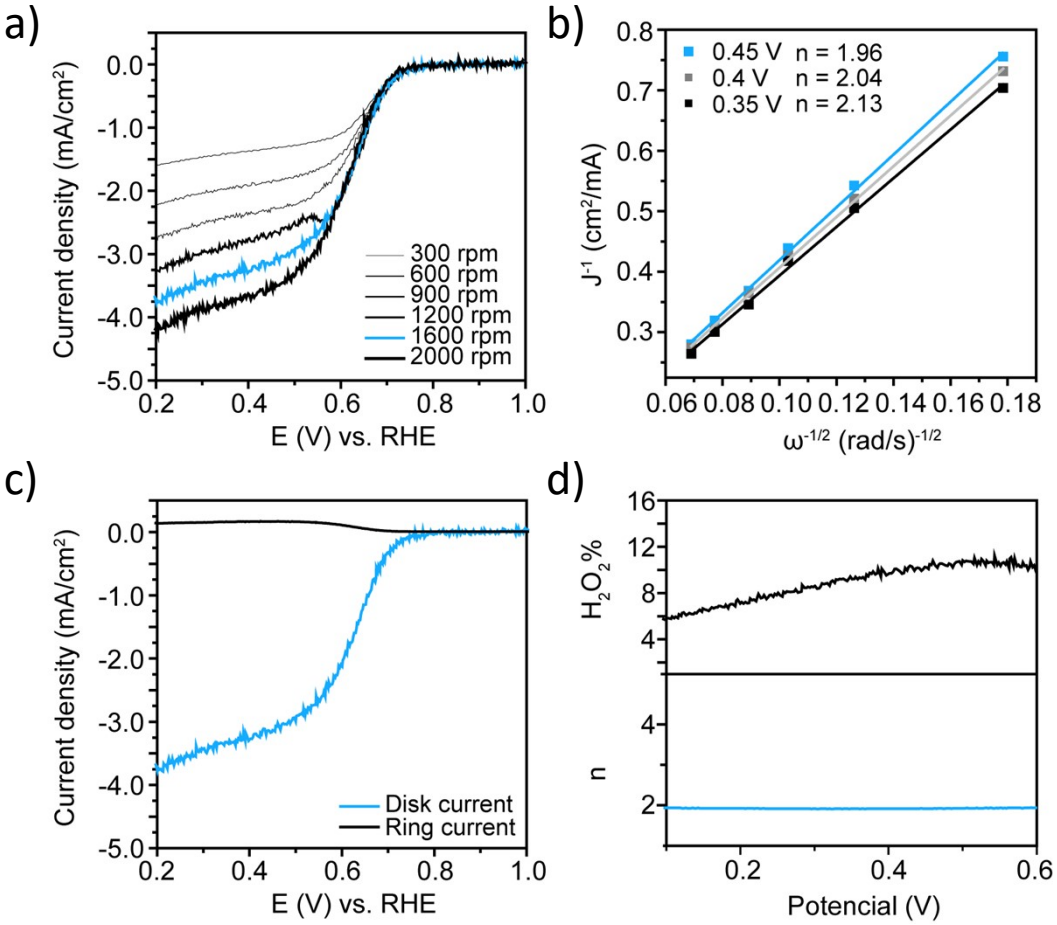

Figure S22. ORR electrochemical characterization for the MINT(6,5)-2 catalyst. a) LSV curves on an RDE with various rotating speeds. b) K–L plots obtained from (a). c) RRDE voltammograms and the corresponding amperometric currents at the ring (dark line) and the disk (light line) electrodes. The electrode rotation rate was 1600 rpm, and the Pt ring electrode was 1.2 V vs. RHE. d) HO_2^- production yields and n values derived from the disk and ring currents. Measurements were performed in an O_2 saturated 0.1 M NaOH aqueous solution at the scan rate of 5 mV s^{-1}.

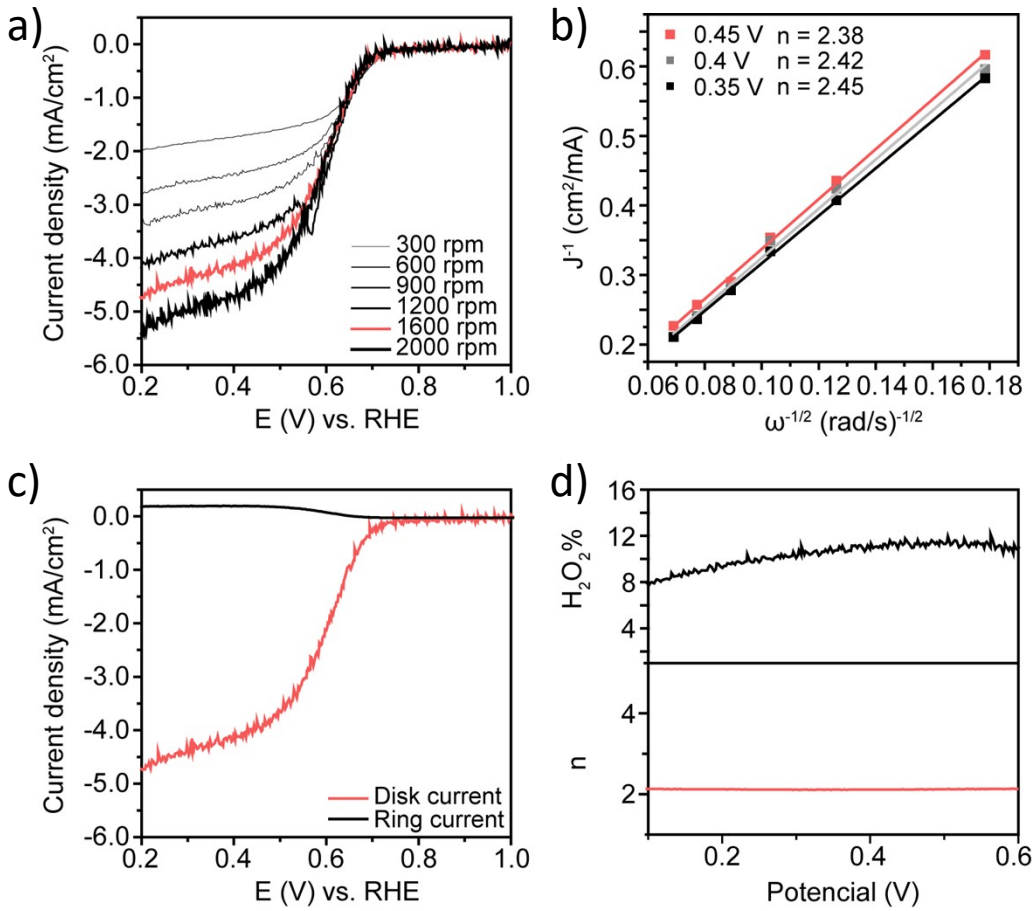

Figure S23. ORR electrochemical characterization for the MINT(7,6)-1 catalyst. a) LSV curves on an RDE with various rotating speeds. b) K–L plots obtained from (a). c) RRDE voltammograms and the corresponding amperometric current at the ring (dark line) and the disk (light line) electrode. The electrode rotation rate was 1600 rpm, and the Pt ring electrode was 1.2 V vs. RHE. d) HO_2^- production yields and n values derived from the disk and ring currents. Measurements were performed in an O_2 saturated 0.1 M NaOH aqueous solution at the scan rate of 5 mV s^{-1}.

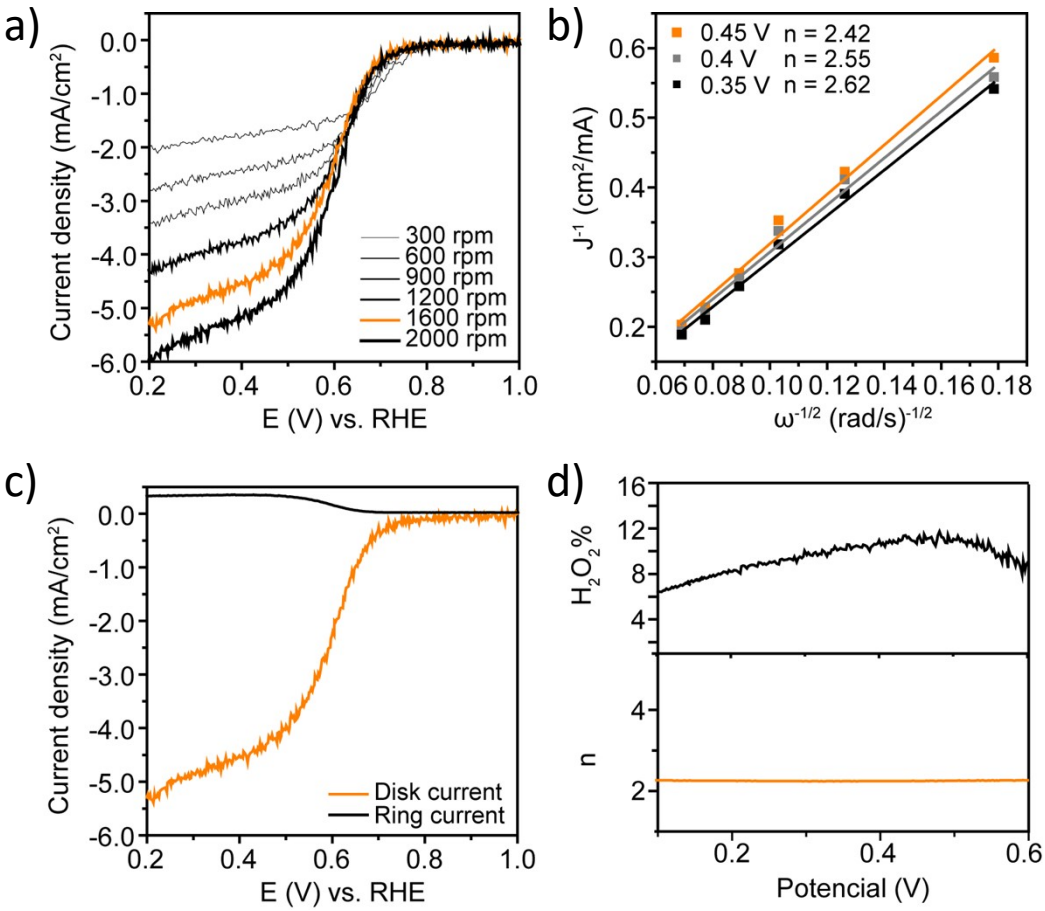

Figure S24. ORR electrochemical characterization for the MINT(7,6)-2 catalyst. a) LSV curves on an RDE with various rotating speeds. b) K–L plots obtained from (a). c) RRDE voltammograms and the corresponding amperometric currents for ORR at the ring (dark line) and the disk (light line) electrode. The electrode rotation rate was 1600 rpm, and the Pt ring electrode was 1.2 V vs. RHE. d) HO_2^- production yields and n values derived from the disk and ring currents. Measurements were performed in an O_2 saturated 0.1 M NaOH aqueous solution at the scan rate of 5 mV s^{-1}.

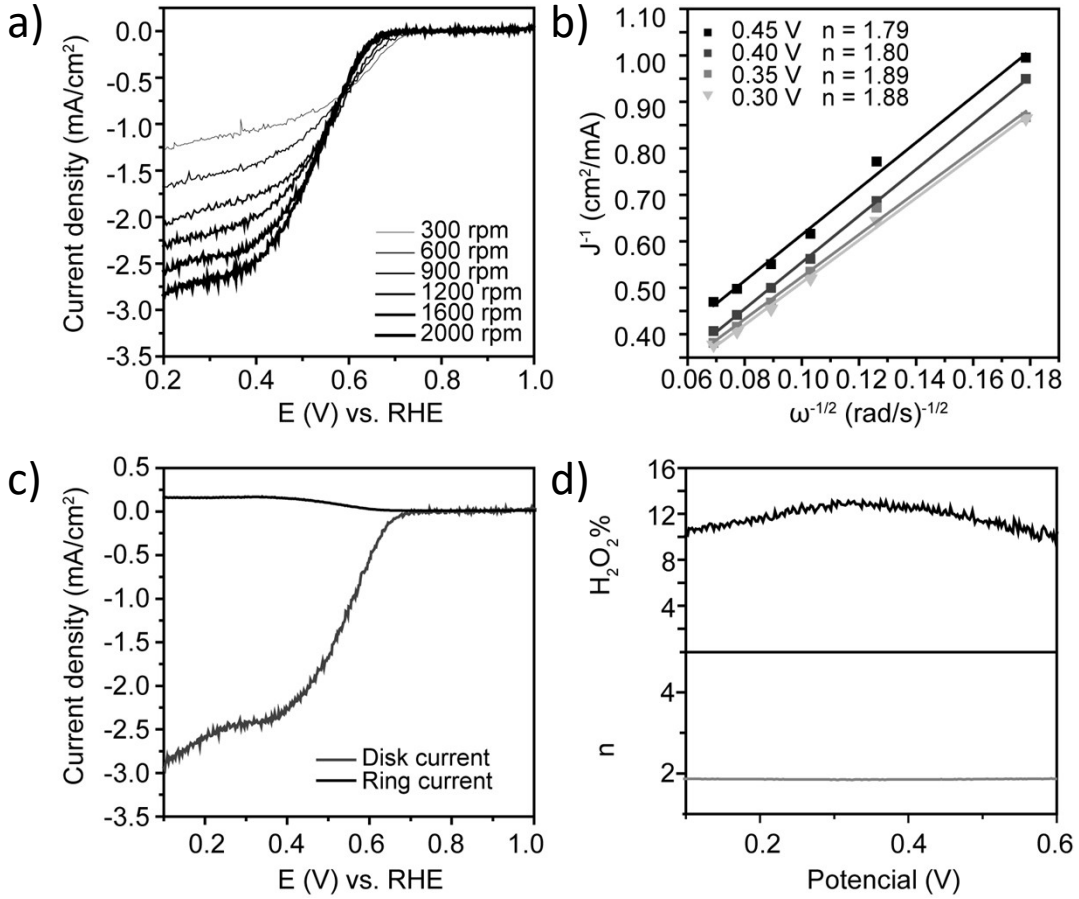

Figure S25. ORR electrochemical characterization for the (6,5)-SWNT catalyst. a) LSV curves on an RDE with various rotating speeds. b) K–L plots obtained from (a). c) RRDE voltammograms and the corresponding amperometric currents at the ring (dark line) and the disk (light line) electrodes. The electrode rotation rate was 1600 rpm, and the Pt ring electrode was 1.2 V vs. RHE. d) HO_2^- production yields and n values derived from the disk and ring currents. Measurements were performed in an O_2 saturated 0.1 M NaOH aqueous solution at the scan rate of 5 mV s^{-1}.

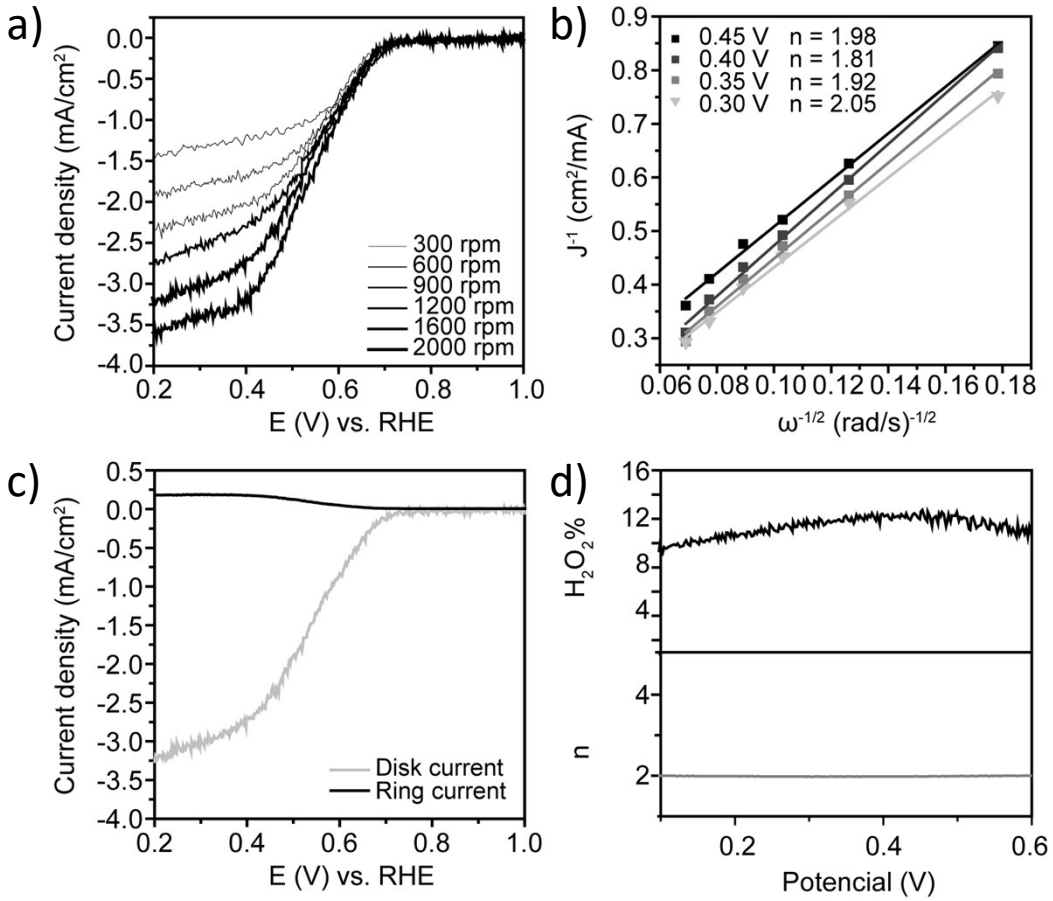

Figure S26. ORR electrochemical characterization for the (7,6)-SWNT catalyst. a) LSV curves on an RDE with various rotating speeds. b) K–L plots obtained from (a). c) RRDE voltammograms and the corresponding amperometric currents for ORR at the ring (dark line) and the disk (light line) electrodes. The electrode rotation rate was 1600 rpm, and the Pt ring electrode was 1.2 V vs. RHE. d) HO_2^- production yields and n values derived from the disk and ring currents. Measurements were performed in an O_2 saturated 0.1 M NaOH aqueous solution at the scan rate of 5 mV s^{-1}.

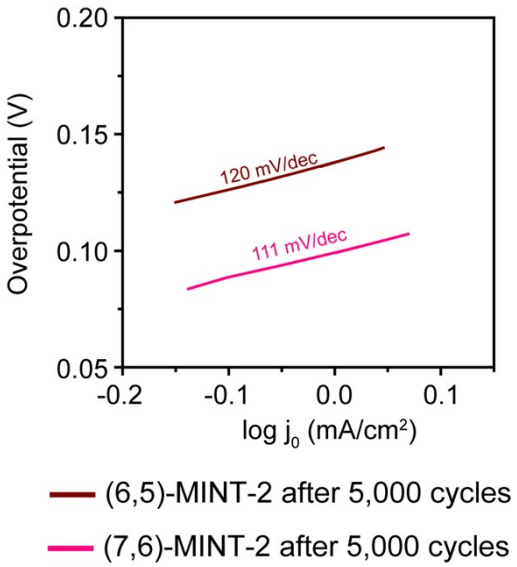

Figure S27. Tafel plots after stability 5,000 ORR cycles.

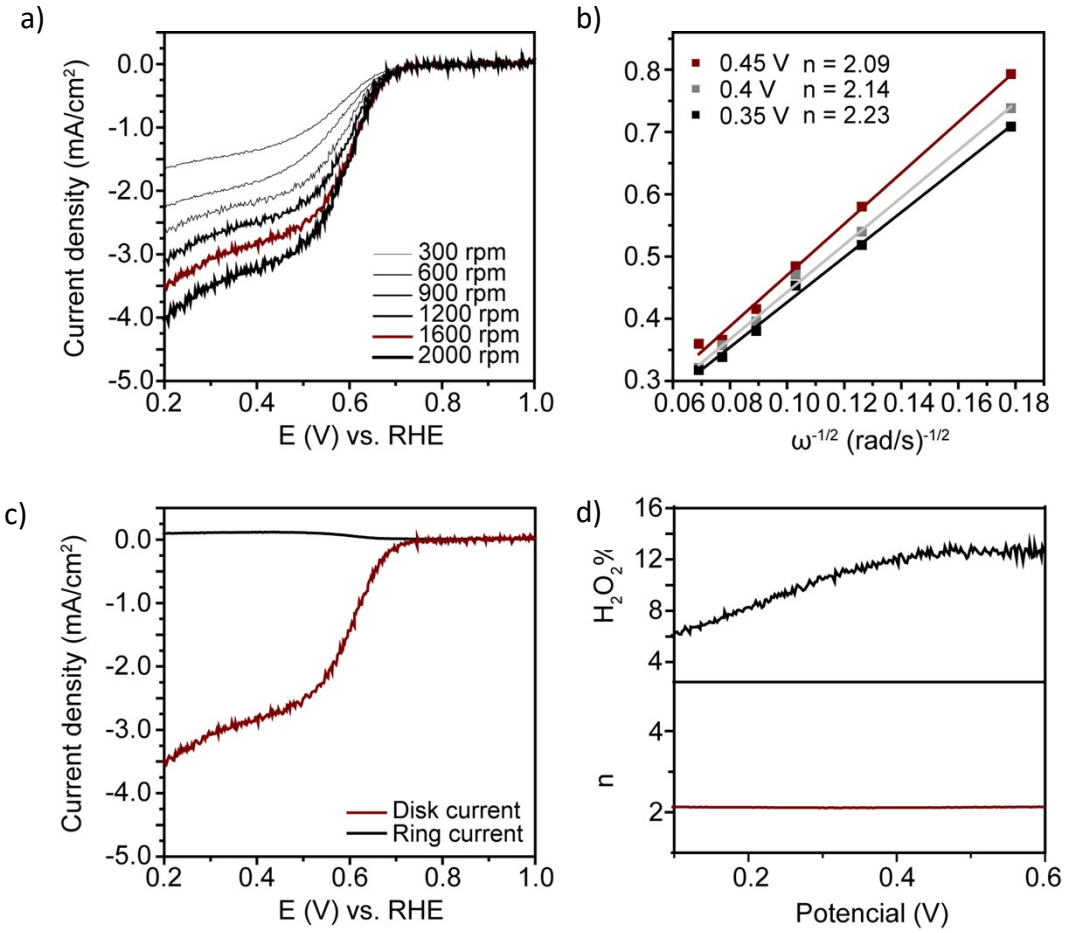

Figure S28. ORR electrochemical characterization for the MINT(6,5)-2 electrode after 5,000 ORR cycles. A) LSV curves on an RDE with various rotating speeds. B) K–L plots obtained from (a). c) RRDE voltammograms and the corresponding amperometric currents for ORR at the ring (dark line) and the disk (light line) electrodes. The electrode rotation rate was 1600 rpm, and the Pt ring electrode was 1.2 V vs. RHE. D) HO_2^- production yields and n values derived from the disk and ring currents. Measurements were performed in an O_2 saturated 0.1 M NaOH aqueous solution at the scan rate of 5 mV s^{-1}.

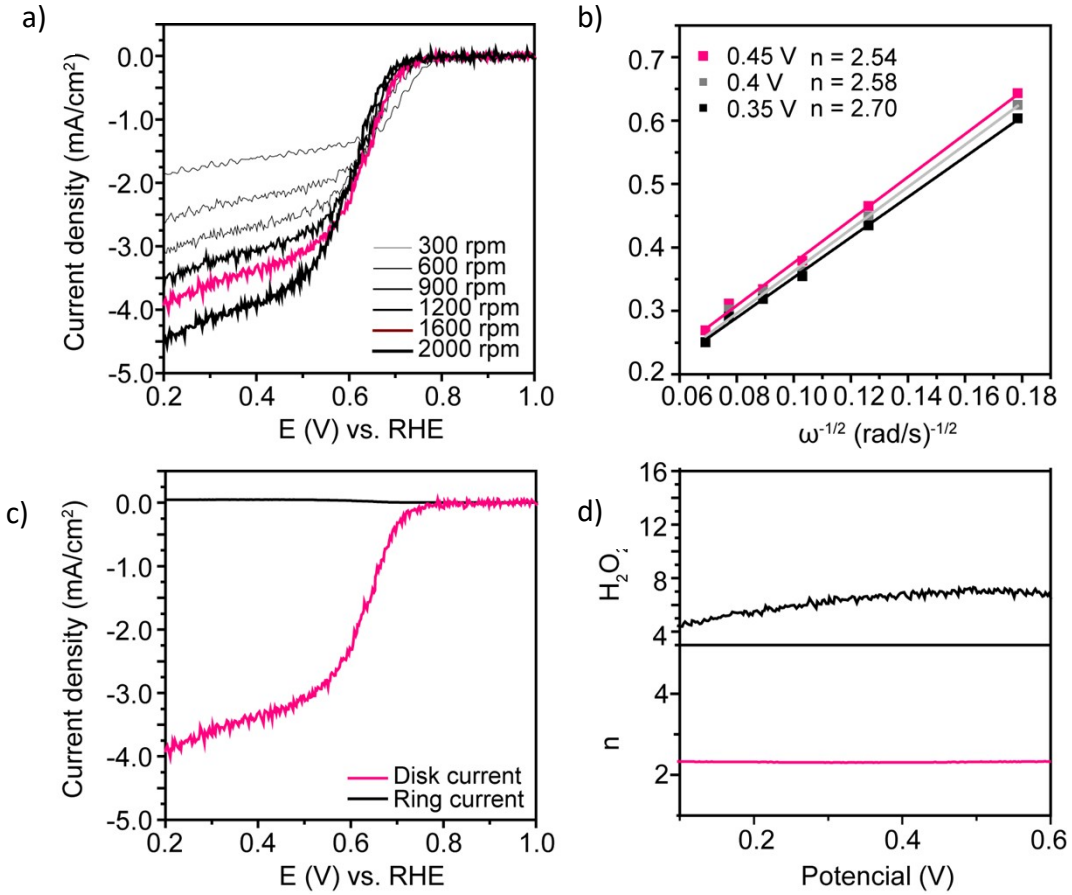

Figure S29. ORR electrochemical characterization for the MINT(7,6)-2 electrode after 5,000 ORR cycles. a) LSV curves on an RDE with various rotating speeds. B) K–L plots obtained from (a). c) RRDE voltammograms and the corresponding amperometric currents for ORR at the ring (dark line) and the disk (light line) electrodes. The electrode rotation rate was 1600 rpm, and the Pt ring electrode was 1.2 V vs. RHE. D) HO_2^- production yields and n values derived from the disk and ring currents. Measurements were performed in an O_2 saturated 0.1 M NaOH aqueous solution at the scan rate of 5 mV s^{-1}.

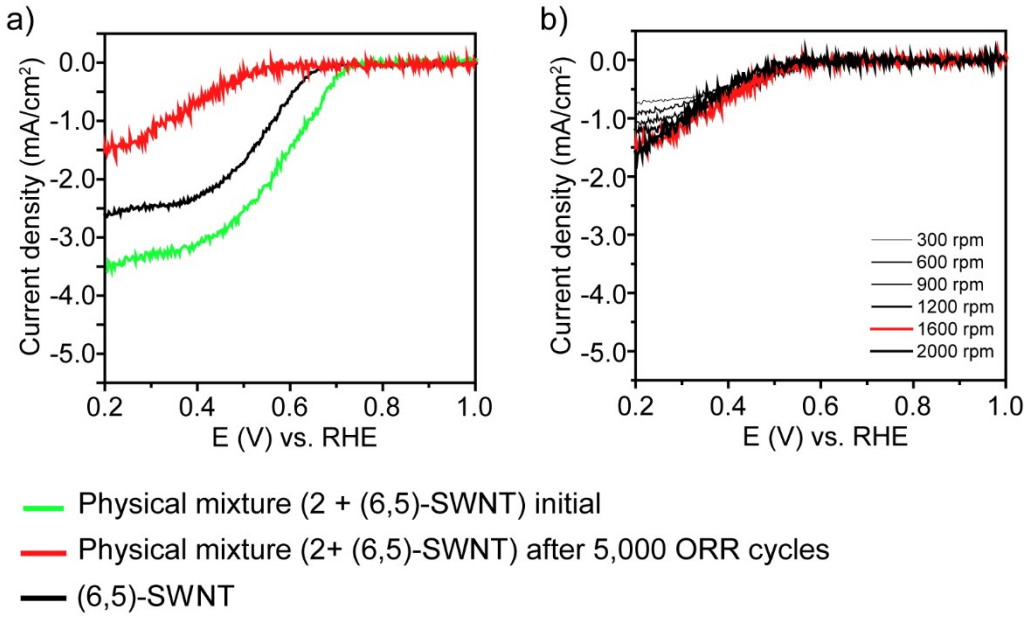

Figure S30. For the **physical mixture (2 + (6,5)-SWNT)** a) a comparison of the ohmic drop corrected ORR polarization curves for the initial sample and after 5,000 ORR cycles and b) LSV curves on an RDE with various rotating speeds after 5,000 ORR cycles. Measurements were performed in an O_2 saturated 0.1 M NaOH aqueous solution at the scan rate of 5 mV s^{-1}.

Table S6. ORR electro-kinetic parameter values for the physical mixture **(2 + (6,5)-SWNT)** initial sample and after 5,000 ORR cycles.

Catalyst	**Half-Wave Potential ($E_{1/2}$, V *vs.* RHE)**	**Onset potential (E_{onset}, V *vs.* RHE)**	**Current density j_L at 0.2 V (mA/cm^2)**
Physical mixture **(2 + (6,5)-SWNT)** initial	0.56	0.73	3.5
Physical mixture **(2 + (6,5)-SWNT)** after 5,000 ORR cycles	0.42	0.55	1.5

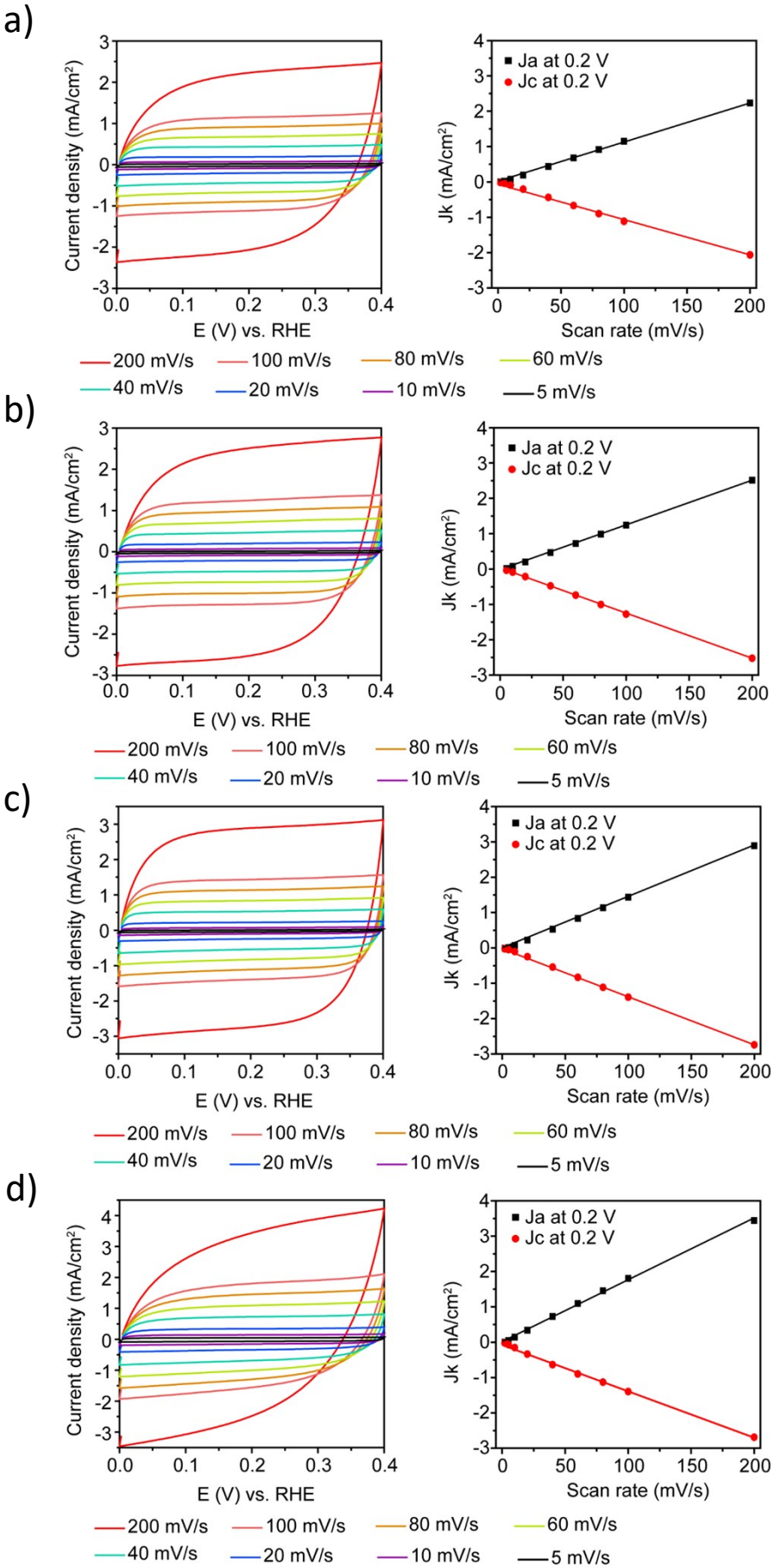
a)
b)
c)
d)
Current density (mA/cm²)
E (V) vs. RHE
Jk (mA/cm²)
Scan rate (mV/s)
Ja at 0.2 V
Jc at 0.2 V
200 mV/s
100 mV/s
80 mV/s
60 mV/s
40 mV/s
20 mV/s
10 mV/s
5 mV/s

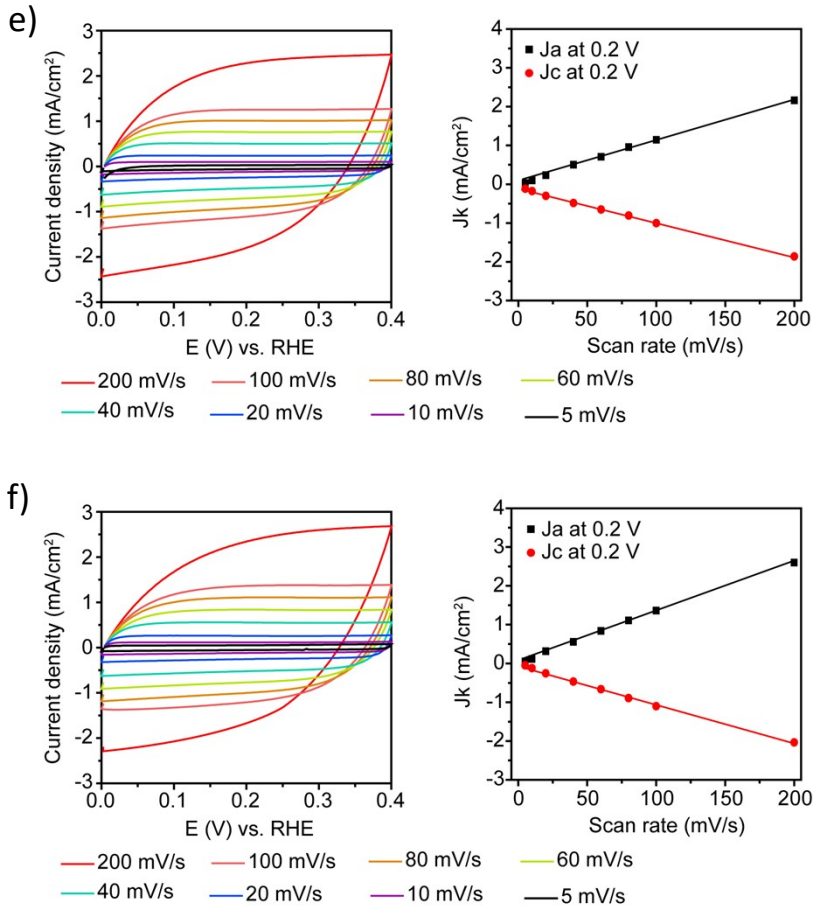

Figure S31. Capacitative current densities at various scan rates and the variation of the kinetic anodic and cathodic currents with the scan rate for a) **MINT(6,5)-1**, b) **MINT(6,5)-2**, c) **MINT(7,6)-1**, d) **MINT(7,6)-2**, e) **(6,5)-SWNT** and f) **(7,6)-SWNT**.

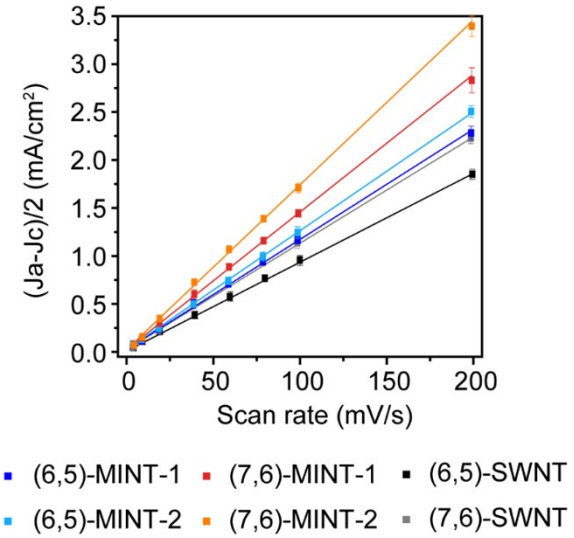

Figure S32. Plots of the capacitative current densities difference at 0.2 V vs. RHE as a function of the scan rate to estimate the C_{dl} from the slope for a fixed electrode surface area.

Table S7. The double-layer capacitance values of the MINTs and SWNTs in this work.

	MINT(6,5)-1	MINT(6,5)-2	MINT(7,6)-1	MINT(7,6)-2	6,5-SWNT	7,6-SWNT
Double-layer capacitance (Cdl) (mF/cm^2)	**10.98 ± 0.36**	**12.47 ± 0.29**	**14.03 ± 0.78**	**14.91 ± 0.61**	**9.14 ± 0.21**	**10.10 ± 0.24**

References

1. Y. Y. Li, F. Y. Cheng, J. N. Zhang, Z. M. Chen, Q. Xu and S. J. Guo, Small 2016, 12, 2839-2845.
2. Z. Sadighi, J. Liu, L. Zhao, F. Ciucci, J.-K. Kim, Nanoscale 2018, 10, 22549-22559